

EUTECTIC AND PERITECTIC EQUILIBRIA IN  
COHERENT BINARY ALLOYS

by

Samiah Hassan

---

Copyright © Samiah Hassan 2025

A Thesis Submitted to the Faculty of the  
DEPARTMENT OF MATERIALS SCIENCE AND ENGINEERING

In Partial Fulfillment of the Requirements  
For the Degree of

MASTER OF SCIENCE

In the Graduate College  
THE UNIVERSITY OF ARIZONA

2025

THE UNIVERSITY OF ARIZONA  
GRADUATE COLLEGE

As members of the Master’s Committee, we certify that we have read the thesis prepared by: **Samiah Hassan**  
titled:

and recommend that it be accepted as fulfilling the thesis requirement for the Master’s Degree.

*M. Latypov*

Marat Latypov

Date: Apr 28, 2025

*Pierre Deymier*

Pierre Deymier

Date: Apr 29, 2025


*KMU*

[Krishna Muralidharan \(Apr 29, 2025 09:18 PDT\)](#)

Krishna Muralidharan

Date: Apr 29, 2025

Final approval and acceptance of this thesis is contingent upon the candidate’s submission of the final copies of the thesis to the Graduate College.

I hereby certify that I have read this thesis prepared under my direction and recommend that it be accepted as fulfilling the Master’s requirement. 

*M. Latypov*

Marat Latypov

Thesis Committee Chair

Department of Materials Science and Engineering

Date: Apr 28, 2025

ARIZONA

## Acknowledgment

I want to express my deep gratitude to my advisor, Marat I. Latypov, for his continuous support, guidance, and encouragement throughout the course of this research. His expertise, patience, and mentorship have played a vital role in the development of this thesis and in my growth as a graduate student.

I would also like to extend my heartfelt thanks to Pierre Deymier and Krishna Muralidharan, members of my thesis committee, for their thoughtful feedback, valuable insights, and kind support, which have greatly enriched the quality of my work.

A special thank you to Elsa Morales, my Graduate Advisor, for her consistent guidance and advice during my academic journey at University of Arizona.

Lastly, I am deeply thankful to my parents and friends for their unwavering encouragement, love, and moral support throughout this journey. Their belief in me has been a constant source of strength and motivation.

## **Dedication**

I dedicate this thesis to my parents, family, and teachers who have supported me during my academic journey. Their contributions are as significant as mine in this work.

# Table of Content

1	Introduction . . . . .	8
1.1	Phase diagram . . . . .	9
1.2	Phase Equilibria map . . . . .	10
1.3	Gibbs Energy . . . . .	11
1.4	Gibbs Phase Rule . . . . .	13
1.5	Common tangent . . . . .	14
1.6	Lattice structure and lattice mismatch . . . . .	15
1.7	Coherent binary alloy . . . . .	18
1.8	Eutectic and Peritectic phase equilibria . . . . .	19
1.9	Lagrange Multipliers . . . . .	20
2	CALPHAD . . . . .	23
3	Motivation . . . . .	24
4	Theoretical model . . . . .	26
5	Case studies . . . . .	30
5.1	General approach and specific functional forms of Gibbs free energies .	30
5.2	Computer implementation . . . . .	31
5.3	Case study 1: Eutectic system . . . . .	32
5.4	Case study 2: Peritectic system . . . . .	35
5.5	Application of lever-rule on phase equilibria map . . . . .	39
5.6	Comparative Analysis with CALPHAD for Cu–Ag Alloy . . . . .	41
6	Discussion . . . . .	43
7	Conclusion . . . . .	46

## List of Tables

1	Comparison between Phase Diagram and Phase equilibria maps . . . . .	11
2	Comparison between Eutectic and Peritectic Equilibria [1, 2] . . . . .	20
3	Parameters for Eutectic system for the Gibbs energy function . . . . .	32
4	Parameters for Peritectic system for the Gibbs energy function . . . . .	36

## List of Figures

1	Free energy as a function of the arrangements of atoms in phases. A: stable configuration, B: metastable configuration [3] . . . . .	12
2	Common tangent method applied to two phases, $\alpha$ and $\beta$ , for a binary system A-B (adapted from [4]) . . . . .	14
3	Different types of crystal structures . . . . .	16
4	The epitaxial layer in the presence of lattice mismatch between the layer material and the substrate material. The case of purely elastic accommodation of strain is presented (no misfit dislocations) [5] . . . . .	17
5	(a) Eutectic and (b) Peritectic phase equilibria maps in binary alloy considering arbitrary values of temperature and composition . . . . .	19
6	Lagrange Multiplier method [6, 7, 8, 9] . . . . .	21
7	Gibbs free energy curve under different coherency stress for Eutectic Binary-phase equilibria for below, at, and above Eutectic temperature ( $T_E$ ) . . . . .	33
8	Magnified projection of Gibbs energy curves for the three-phase region ( $\alpha$ - $\beta$ - $L$ ) curve under coherency stress level 2.5. . . . .	34
9	Eutectic Binary-phase equilibrium map under different coherency stresses . . . . .	35
10	Gibbs free energy curve under different coherency stress for Peritectic Binary-phase equilibria for below, at, and above Peritectic temperature ( $T_P$ ) . . . . .	37
11	Peritectic Binary-phase equilibrium map under different coherency stresses . . . . .	38
12	Calculated $\beta$ - $L$ Phase Boundaries (blue dashed line: $L$ phase boundary, black dashed line: $\beta$ phase boundary) . . . . .	39
13	Application of lever rule on Peritectic phase equilibria map ( $W= 2.5$ ) . . . . .	40
14	Comparative Analysis of the theoretical model for Cu-Ag Alloy . . . . .	41
15	Deviation of stressed combination of phases vs non-stressed represented by tangent line . . . . .	42

## Abstract

Phase equilibria in a coherent binary alloy for the eutectic and peritectic systems are analyzed in this study to construct a theoretical model that will provide conditions for three-phase equilibrium in the presence of coherency stress between the solid phases. Our analysis employs simple quadratic functions for the Gibbs energy for individual phases, considering the solid phases to be temperature-independent. To facilitate an analytical solution, we used simplified assumptions about the system, explicitly considering an infinite volume occupied by three phases and the solid phases being isotropic and linearly elastic. We use a mathematical optimization method, Lagrange multiplier, to minimize the functions of Gibbs free energy subject to the constraints of volume fractions and phase compositions that satisfy the equilibrium conditions. This theoretical study demonstrates the effect of coherency stress on invariant points of phase diagrams, including a liquid leveraging the original Larche-Cahn formulation to evaluate the impact of coherency stress on eutectic and peritectic points in binary alloys. The common tangent construction is not applicable in the presence of strain energy between the solids, and the Gibbs phase rule no longer holds. Our findings demonstrated that coherency stress has distinct consequences on the eutectic and peritectic equilibria due to the difference in compositions between one solid and liquid phase and the difference in the melting points of the solid phases; therefore, instead of forming the three-phase region, usual to eutectic equilibria, a two-phase region with one solid and liquid becomes more dominant in the peritectic equilibria.

# 1 Introduction

The properties of metallic alloys depend on their microstructures developing due to transformations occurring throughout their production processes, such as solidification, thermo-mechanical treatments, and heat treatments. Equilibrium composition–temperature phase diagrams for atmospheric pressure are the starting point for understanding how microstructures develop during most processing. However, useful microstructures are often far from stability, and an understanding of the thermodynamic foundation of phase diagrams for stable and metastable equilibrium increases their efficacy [4]. The phase diagram provides an illustrated form to understand the conditions of phase transformations. Phase transformations play an important role in materials science in determining the characteristics of materials under different conditions. It is concerned with the thermodynamic equilibrium of the system. Understanding the basic concept of the phase diagram is essential, which is the beginning of wisdom for different material systems [10]. It illustrates the equilibrium state of a thermodynamic system, indicating the existence of one phase, the coexistence of two or three phases at a specific temperature and pressure, and the anticipated phase transformations. This critical phenomenon can be identified by phase transformation, the most effective method for creating various microstructures to understand the fundamental properties of materials; for instance, heating and rapidly cooling steel (quenching) transforms its internal structure, creating a harder, stronger material.

Phase diagrams are fundamental tools in materials design. They provide equilibrium maps that define the stable phases of alloys under different temperatures, pressures, and compositions. By identifying the conditions under which desired phases form, phase diagrams are essential for optimizing mechanical properties such as strength, ductility, and corrosion resistance. The development of phase diagrams is based mainly on experimental measurements and thermodynamic modeling. While phase diagrams describe equilibrium behavior, real-world processes like alloy solidification and crystal growth often involve non-equilibrium effects that should be analyzed relative to these diagrams. The CALPHAD (Computer Coupling of Phase Diagrams) approach is the most familiar, integrating both experimental outcomes and thermodynamic modeling to provide a complete computational tool to forecast the phase behavior. This method mainly depends on minimizing the Gibbs Free energy to find the most stable phase for a given composition and temperature, enabling the detailed estimation of the systems compatible with thermodynamic principles [11].

Our study analyzes the eutectic and peritectic equilibria of a coherent binary alloy by minimizing the relevant phases' thermodynamic potential, specifically the Gibbs free energy, at given temperatures. This approach allows us to predict stable phase formations and transformations, providing deeper insight into the thermodynamic equilibrium of a coherent system under stress.

## 1.1 Phase diagram

Phase diagrams are the foundation for performing basic materials research in solidification, crystal growth, joining, solid-state reaction, phase transformation, oxidation, etc. On the other hand, a phase diagram also serves as a road map for materials design and process optimization since it is the starting point in manipulating processing variables to achieve the desired microstructures. Until the last decade of the 20th century, phase diagrams were determined primarily by meticulous and costly experimentation.[12]

Phase diagrams are a cornerstone of knowledge in materials science and engineering. They serve as critical guides for designing various materials, including alloys, ceramics, semiconductors, cement, concrete, and any other material where the concept of phases is relevant.[10] The properties of materials are related to their microstructure, and the microstructure is associated with the constitution, which states the number of phases present, their proportion, and their composition. To determine the constitution, we need to know the phase diagram. Typically, in a solid, microstructure consists of grains of phases against one another. These grains may consist of only one phase, a single-phase microstructure, or grains of many phases, a polyphase microstructure. An inspection of a material's overall properties may proceed by determining the constitution of the phases involved and combining this with the knowledge of their specific properties, such as crystal structures, physical properties, etc., later. Very importantly, it incorporates knowledge of the distribution of the phases in the microstructure. They can help determine the shapes and sizes of the grains, how they fit together, and how they interact. The information that allows us to predict the constitution from a graphical plot of the phases involved is known as a phase diagram, a function of what kind of a phase diagram is used for a given material. The independent state variables that control the phases in a given diagram are the number of components involved, the proportion of the components in the material, the temperature, and the external pressure. Simple phase diagrams generally involve only two state vari-

ables: temperature and composition. If one is plotted vertically and the other horizontally, a graphical representation shows the distribution of the various possible phase fields allowed by the two variables. All materials exist in three forms: gaseous, liquid, or solid, typically called phases. These phases depend on the conditions of the state, meaning the values of the relevant state variables. The term "phase" refers to a region of space occupied by a uniform material. Each single-phase area is depicted graphically in a phase diagram and usually labeled with a single term. Engineers often find it convenient to use this label to refer to all the material associated with that field, regardless of how the physical properties may vary within different parts of the field. As a result, in engineering practice, the distinction between "phase" and "phase field" is often overlooked, and all materials sharing the same phase name are typically referred to as the same "phase".[12]

Phase diagram is a graphical representation of the physical states of a substance under different conditions of temperature and pressure. It typically plots pressure on the vertical axis against temperature on the horizontal axis, illustrating the stability regions for other phases. The boundaries between these regions, represented by lines or curves on the diagram, indicate the conditions under which phases transform from one to another. At these boundaries, two phases can coexist in equilibrium as well. Phase diagram is a graphical representation of the physical states of a substance under different conditions of temperature and pressure. It typically plots pressure on the vertical axis against temperature on the horizontal axis, illustrating the stability regions for other phases. Other than that, it plots temperature on the vertical axis and composition on the horizontal axis to understand how the composition of the binary or multicomponent system influences phase stability at different temperatures. Each region in this diagram represents a phase or a combination of stable phases under specific compositional and temperature conditions. The boundaries between these regions, represented by lines or curves on the diagram, indicate the conditions under which phases transform from one to another. At these boundaries, two phases can coexist in equilibrium as well.[12]

## 1.2 Phase Equilibria map

In our study, we use the term 'Phase Equilibria Map' instead of 'phase diagram.' Though both of them identify the phases that are stable, there is a distinct difference between the two. While the phase diagram can give a quantitative estimation of the composition of

the phases following the lever rule- a formula used to determine the mole fraction or the mass fraction of each phase of a binary equilibrium phase diagram, the 'phase equilibria map' does not adhere to those lever rule guidelines. Therefore, we will focus on a simplified qualitative analysis of the phases and refer to it as a 'Phase Equilibria Map.'

The basic differences between the 'Phase diagram' and 'phase equilibria maps' are shown in Table 1.

Table 1: Comparison between Phase Diagram and Phase equilibria maps

<b>Phase diagram</b>	<b>Phase equilibria maps</b>
Graphical representation showing stable phases at different conditions (temperature, pressure, composition).	Graphical representation showing phases in equilibrium under various conditions without detailing phase proportions.
Understanding how different phases form and interact under various conditions and calculating proportions of each phase.	Identifying stable phases under specific conditions without quantifying their proportions.
Provides Lever Rule to calculate the portion of phases in a two-phase region.	Lever Rule or similar quantitative measures are not applicable.

### 1.3 Gibbs Energy

There are three states of equilibrium: stable, metastable, and unstable. These three conditions are illustrated schematically in a structural sense in Figure 1. Stable equilibrium occurs when the object is in its lowest energy state. Metastable equilibrium exists when additional energy ( $\Delta G$ ) must be applied before the object can reach proper stability. An unstable equilibrium exists when no additional energy is needed before reaching metastability or stability. Although stable equilibrium conditions seldom exist in real everyday materials, studying equilibrium systems is highly valuable because they provide a limiting condition from which actual conditions can be estimated. The state variables that are selected to control a given system determine the free energy values of all the possible phases that can

exist in that system for all possible combinations of the variables. The phases represented in a phase diagram represent the lowest free energy value at each state point. [3]

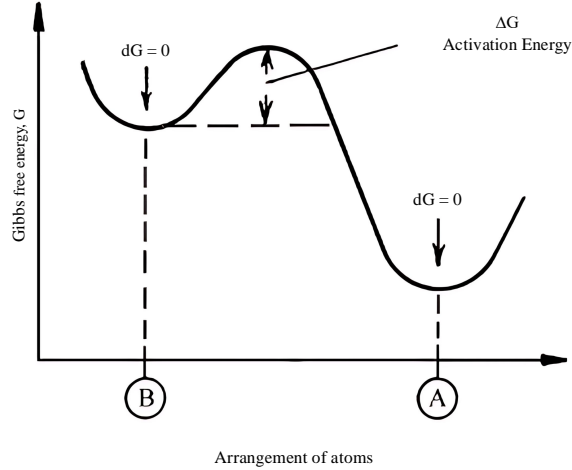


Figure 1: Free energy as a function of the arrangements of atoms in phases. A: stable configuration, B: metastable configuration [3]

Gibbs Energy ( $G$ ), also known as Gibbs Free Energy, is associated with the energy available to do work and determines whether a reaction will be spontaneous. Like the universe, every system wants to be stable by giving off energy, which will cause the system to have a negative enthalpy change. On the other hand, the universe also wants to be disordered, increasing entropy. Fulfilling these two conditions, the change in free energy will be negative, and the reactions will be spontaneous on all values of temperatures. If the  $\Delta G$  is positive, the reaction needs external energy to proceed, and the reaction will not be spontaneous.[13]. Gibbs Free Energy is a thermodynamic potential representing the maximum reversible work a thermodynamic system can perform at specific conditions, like temperature and pressure. It is essential for predicting spontaneity and stability in chemical reactions and phase transformations. Gibbs's free energy is mathematically determined by subtracting the product of temperature and entropy change from the enthalpy change, as presented in Eq. 1.

$$\Delta G = \Delta H - T\Delta S \quad (1)$$

where  $\Delta H$  denotes the enthalpy,  $T$  is the absolute temperature, and  $\Delta S$  represents the entropy of the system, is the extent of the disorder of a system describing how much energy is not available to do work. The more disordered a system is and the higher the entropy, the less energy is available to do work. A negative Gibbs energy change ( $\Delta G < 0$ ) indicates that a reaction or process occurs spontaneously, whereas a positive Gibbs energy change ( $\Delta G > 0$ ) indicates non-spontaneity, requiring external energy input. Equilibrium corresponds to a Gibbs energy minimum, i.e., when  $\Delta G = 0$ . In thermodynamics, the alloy's phase or combination of phases with the minimum Gibbs free energy at constant temperature, pressure, and composition is the most stable. It will be observed at equilibrium, showing the direct connection of stability or equilibrium of the phases with the minimized Gibbs free energy. So, in materials science, Gibbs's free energy is considered an essential aspect in anticipating the microstructural development and materials synthesis conditions by handling phase stability, phase diagrams, and equilibrium compositions. In our current work, our initial approach is to minimize the Gibbs free energy of coherent binary alloys to obtain phase equilibria.

#### 1.4 Gibbs Phase Rule

Gibbs Phase Rule provides a fundamental framework for comprehending the degrees of freedom in a multiphase chemical system at equilibrium. The rule is compulsory in materials science and chemical engineering, offering an essential understanding of phase behavior and phase transitions. Different phases in a system have the same temperature and pressure as the requirements for equilibrium. Further, each component has the same chemical potential in all the phases in equilibrium. This is derived from the Gibbs phase rule, which states that [12]

$$F = C - P + 2$$

where  $F$  is the minimum number of degrees of freedom required to reproduce the system,  $C$  represents the number of independent components, and  $P$  refers to the number of phases. The Gibbs phase rule applies to multicomponent macro systems in determining the number of phases at a given temperature and pressure. Gibbs Phase Rule offers the design and analysis of the synthesis of new materials and the study of phase diagrams and phase transformation. In a binary alloy system, the rule predicts that up to three phases can coexist at equilibrium under certain conditions without changing the system's overall composition

or temperature.

## 1.5 Common tangent

The common tangent method is an essential graphical mechanism to determine equilibrium compositions and phase boundaries within a binary phase diagram. In thermodynamic equilibrium, the chemical potentials of each component in coexisting phases must be equal, which graphically represents the construction of a common tangent line to the Gibbs free energy curves of the respective phases. It helps determine the compositions of phases that are in equilibrium at a specific temperature and pressure, which imitates the phase coexistence regions such as miscibility gaps, eutectics, and solid-solubility limits [4]. Mathematically, the common tangent condition for two phases (for example,  $\alpha$  and  $\beta$ ) at equilibrium can be expressed as:

$$\mu_i^\alpha(T, P, X_i^\alpha) = \mu_i^\beta(T, P, X_i^\beta) \quad \text{for each component } i$$

where  $\mu_i$  denotes the chemical potential,  $T$  temperature,  $P$  pressure, and  $X_i$  the mole fraction of component  $i$ .

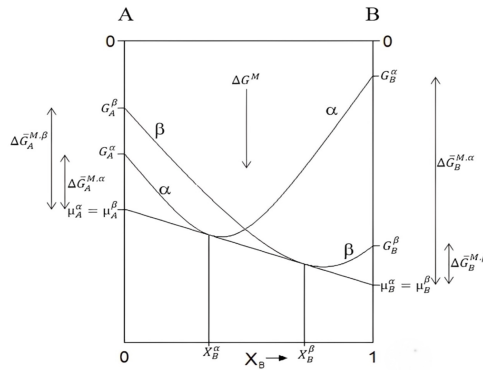


Figure 2: Common tangent method applied to two phases,  $\alpha$  and  $\beta$ , for a binary system A-B (adapted from [4])

Figure 2 illustrates the common tangent method applied to determine phase equilibrium in a binary alloy system showing the Gibbs free energy curves (G) for two phases ( $\alpha$  and  $\beta$ ) as a function of composition (X). Equilibrium between phases is determined by constructing a common tangent line connecting the minimum point of both Gibbs energy curves. At equilibrium, the chemical potentials,  $\mu_i$  of each component (A and B) must be equal in both phases

$$\mu_A^\alpha = \mu_A^\beta = \mu_B^\alpha = \mu_B^\beta$$

This tangent line provides equilibrium compositions of component B in both phases, labeled as  $X_B^\alpha$  and  $X_B^\beta$ . The vertical arrows display the difference in Gibbs free energy between the pure and mixture phases, illustrating the driving force for mixing or separation into distinct phases. This approach is essential in materials science for analyzing alloy phase diagrams and predicting phase stability and transformations. [14]

However, in coherent solids, the common tangent construction is usually invalid as the free energy of the system is not simply the sum of the free energies of the individual phases independent of the position and morphology of the other phases. Coherent phase diagrams can still be formulated by adding the elastic energy of the system to the free energies of the phases in the absence of deformation and then minimizing the resultant energy. This is the recent approach by Williams and Cahn and Larche. [15]

## 1.6 Lattice structure and lattice mismatch

Lattice structures are essential in determining the physical, mechanical, and chemical properties of any type of alloy, such as the impact of lattice structure in our current work for the coherent binary alloy. The lattice structure defines the atomic arrangement within a crystal, directly affecting the behavior of the alloy, interface coherency, and phase equilibrium. Common crystal structures appropriate to binary alloys are as follows:

1. Face-Centered Cubic (FCC): Characterized by atoms positioned at the corners and face centers of the cubic unit cell as shown in Figure 3. FCC alloys generally show high ductility, good corrosion resistance, and superior formability [1].
2. Body-Centered Cubic (BCC): Atoms are at cube corners, with one atom at the center. BCC alloys often exhibit higher strength but lower ductility than FCC alloys, significantly influencing deformation mechanisms and phase stability [1].

3. Hexagonal Close-Packed (HCP): Atoms are arranged in hexagonal layers; these alloys usually maintain limited elasticity and anisotropic mechanical properties, which affects alloy processing and application performance [16].

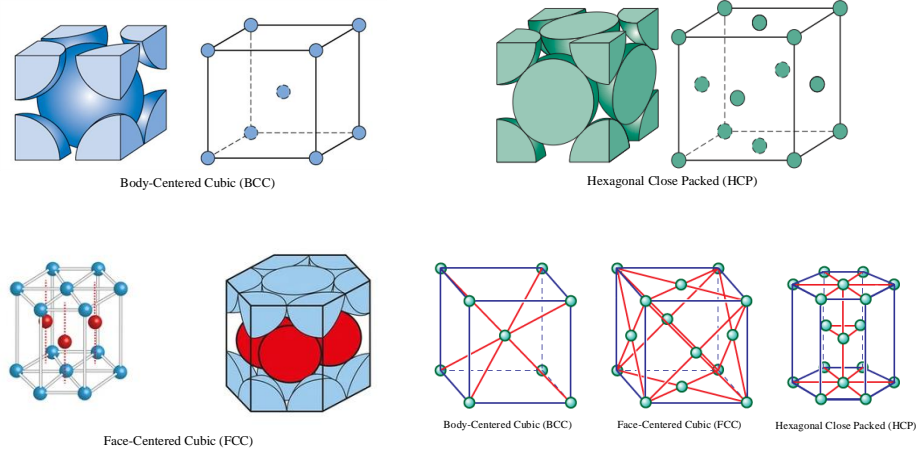


Figure 3: Different types of crystal structures

Lattice mismatch refers to the difference in crystal lattice parameters, precisely the spacing between atoms between two adjacent crystalline materials. This difference typically occurs at interfaces such as between a thin film and its underlying substrate or between consecutively epitaxially grown layers. When two materials with different lattice constants are brought together, the difference affects the mechanical stress at the interface, creating defects such as dislocations or misfit distortions, which significantly influence the material properties. This strain can profoundly affect the behavior of the material, influencing the formation of defects, the quality of epitaxial growth, and the general properties.

Figure 4 depicts the concept of coherency in lattice mismatch between a thin film and its substrate. The diagram illustrates elastic strain accommodation, where the film deforms to match the lattice constant of the substrate at the interface without forming dislocations. The substrate remains rigid while the film undergoes in-plane strain, maintaining coherency. The lattice mismatch is calculated from the lattice constants of the epitaxial layers ( $a_{epi}$ ) and the substrate ( $a_{sub}$ ) as defined by Equation (2): [17]

$$\frac{\Delta a}{a_{epi}} = \frac{a_{epi} - a_{sub}}{a_{epi}} \quad (2)$$

This mechanism is key to understanding strain-induced effects in coherent binary alloys. Moreover, lattice mismatch is an essential phenomenon to consider in many fields, such as in semiconductor engineering; for instance, excessive lattice mismatch may degrade device performance by introducing undesirable carrier diffusion or decreasing the epitaxial rate. However, lattice mismatch is critical in designing advanced optoelectronic and quantum devices. So, understanding and controlling lattice mismatch is essential for optimizing alloy properties, device performance, structural integrity, performance of semiconductors, and developed functional materials applications. Lattice mismatch and strain between an epitaxial layer and the substrate are necessary to analyze crystal stability and material quality.

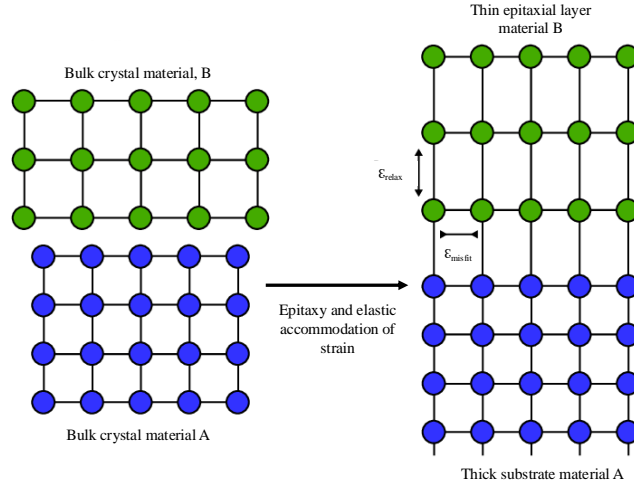


Figure 4: The epitaxial layer in the presence of lattice mismatch between the layer material and the substrate material. The case of purely elastic accommodation of strain is presented (no misfit dislocations) [5]

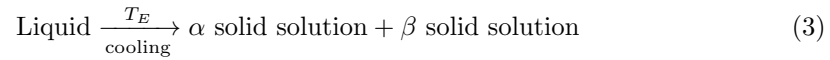
## 1.7 Coherent binary alloy

Binary alloys are composed of two different metal elements, where the elements are combined homogeneously or in specified combinations to form a solid solution, intermetallic compound, or multiphase mixture. In the context of binary alloys, coherency refers to the alignment of the crystal lattice between the precipitate and the surrounding matrix. When the precipitate maintains an identical crystallographic orientation with the matrix, it maintains continuous lattice planes across the interface and is named a coherent precipitate, which minimizes the interfacial energy. Thereby significantly influencing the mechanical properties of the alloy. Sometimes, there is a lattice mismatch between the precipitate and the matrix, which initiates coherency strains. These strains create a stress field that can restrict the movement of the dislocations, changing the mechanical properties of the material. For example, in precipitation-hardened alloys such as the Cu-Al system, coherent precipitates such as Guinier-Preston zones and  $\theta$  phases form with the aluminum matrix, restricting dislocation motion and increasing the strength of the material.

The change in size or composition of the precipitate increases the lattice mismatch, leading to loss of coherency and incoherent precipitates characterized by discontinuous lattice planes with higher interfacial energy. In reality, understanding and maintaining the coherency of precipitates is crucial to the successful application of the alloy or material design for specific domains, as they directly influence the mechanical performance of alloys. Thus, factors such as alloy composition, heat treatment, and processing conditions can be considered to tailor the precipitates' size, distribution, and coherency to achieve the expected mechanical properties of alloys. In coherent binary alloys, the lattice mismatch between constituent phases strongly affects interfacial energy, influencing nucleation and growth processes. Small lattice mismatches tend to have coherent interfaces, minimizing interfacial energies and enhancing mechanical stability. Contrarily, significant lattice mismatches can lead to semi-coherent or incoherent interfaces, generating internal stresses and dislocations, thereby varying the mechanical properties of the alloy [2]. Comprehending the relationship between lattice structures and coherent interfaces allows precise manipulation of alloy properties, which is essential for designing advanced materials for specific engineering applications.

## 1.8 Eutectic and Peritectic phase equilibria

A eutectic equilibrium occurs when a liquid transforms simultaneously into two distinct solid phases at a specific composition and temperature,  $T_E$ , known as the eutectic point, E, as shown in Figure 5 (a). This transformation produces a distinct alternating lamellar or rod-like pattern microstructure, significantly influencing the material's mechanical, thermal, and electrical properties. Eutectic systems are widely studied for their practical importance in alloy design, casting processes, etc.



Upon cooling at the eutectic temperature,  $T_E$ , a liquid phase simultaneously transforms into two distinct solid solutions, denoted as  $\alpha$  and  $\beta$ . This is an invariant reaction because it is in thermal equilibrium. Another way to define this is that the change in Gibbs free energy equals zero, which means the liquid and two solid solutions all coexist together in chemical equilibrium.

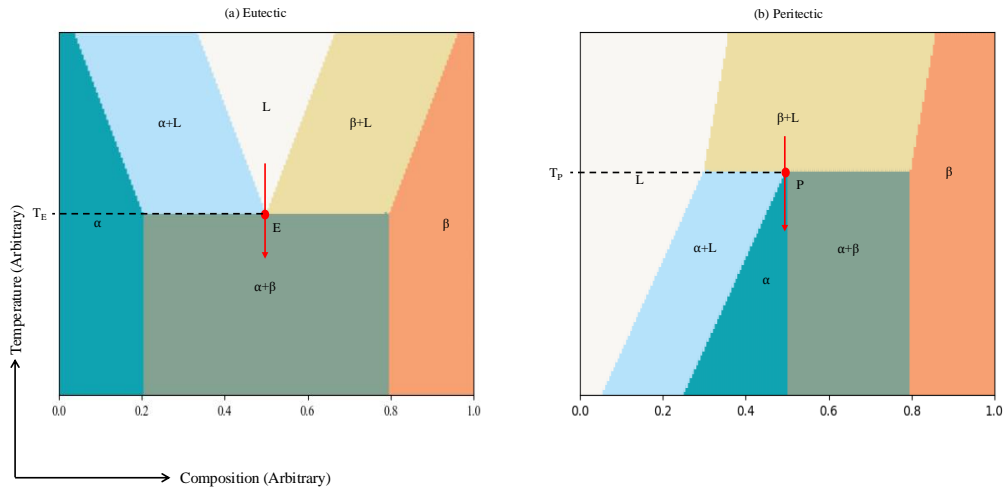
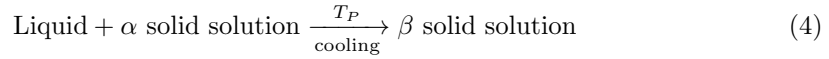


Figure 5: (a) Eutectic and (b) Peritectic phase equilibria maps in binary alloy considering arbitrary values of temperature and composition

However, in the case of peritectic equilibrium, it occurs when a liquid and a solid transform simultaneously into one distinct solid phase at a specific composition and temperature,

$T_P$ , known as the peritectic point, P, as shown in Figure 5 (b). A peritectic equilibrium involves the reaction between a solid,  $\alpha$ , and a liquid phase to form a new, distinct solid phase,  $\beta$ , at a specific peritectic temperature,  $T_P$  and composition. The peritectic transformation generally leads to a complex microstructural transition accompanied by diffusion-controlled mechanisms.



Some fundamental distinctions between eutectic and peritectic equilibria have been shown in Table 2

Table 2: Comparison between Eutectic and Peritectic Equilibria [1, 2]

Feature	Eutectic Equilibrium	Peritectic Equilibrium
<b>Definition</b>	A reaction where a liquid transforms into two (or more) solid phases upon cooling: $L \rightarrow \alpha + \beta$ .	A reaction where a solid phase reacts with a liquid to form a second solid phase upon cooling: $L + \alpha \rightarrow \beta$ .
<b>Phase Diagram</b>	Appears as a "V"-shaped valley where the liquid phase decomposes into two solids at a specified temperature, known as eutectic point.	Appears as a horizontal line where a liquid and a solid react to form a new solid phase at a specified temperature, known as peritectic point.
<b>Composition</b>	The eutectic composition is the specific composition where the liquid transforms directly into two solids without a freezing range.	The peritectic composition is the composition at which the liquid and solid react to form a new solid phase.
<b>Microstructure</b>	Typically results in a lamellar or fibrous two-phase microstructure, e.g., Pb-Sn eutectic.	Peritectic leads to a core-shell or encapsulated microstructure due to incomplete diffusion, e.g., Fe-C system.
<b>Cooling Behavior</b>	The liquid cools to a single temperature where it fully solidifies into two phases.	The liquid and primary solid phase react at a fixed temperature to form a new phase, but complete reaction may not occur due to kinetic limitations.

## 1.9 Lagrange Multipliers

In many applications, the extrema of a function  $f(x,y)$  subject to a constraint  $g(x,y)=k$  must be found out. Such problems are called constrained optimization problems. If the primary function,  $f(x,y)$ , is differentiable along the constraint function,  $g(x,y)$ , the con-

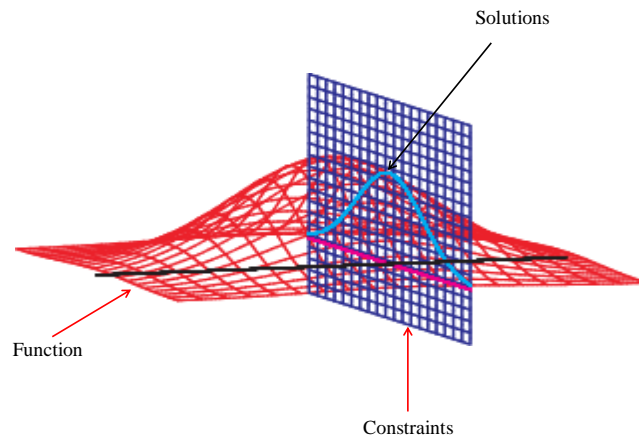


Figure 6: Lagrange Multiplier method [6, 7, 8, 9]

strained optimization problem can be simplified to finding the extrema of a single-variable function derived from the original function along the constraint. In mathematical optimization, Lagrange multipliers, also called Lagrangian multipliers, is a constrained optimization method to get the local maxima and minima of a function,  $f(x,y)$ , subject to constraints,  $g(x,y)$ . In the illustration Figure 6, function  $f$  is shown in red, constraints  $g$  in blue, and the intersection of  $f$  and  $g$  is indicated in light blue is the solution [6, 7, 8, 9].

For an extrema of  $f$  to exist on  $g$ , the gradient of  $f$  must line up with the gradient of  $g$ . If the  $g$  intersects  $f$ , the gradient is a horizontal vector that shows the direction in which the function increases; for  $g$ , it is perpendicular to the curve. If the two gradients of  $f$  and  $g$  are in the same direction, then one is a multiple ( $-\lambda$ ) of the other, so

$$\nabla f = -\lambda \nabla g.$$

The two vectors are equal, so all of their components are as well, giving

$$\frac{\partial f}{\partial x_k} + \lambda \frac{\partial g}{\partial x_k} = 0$$

for all  $k = 1, \dots, n$ , where the constant  $\lambda$  is called the Lagrange multiplier.

The extrema are then found by solving the  $n + 1$  equations in  $n + 1$  unknowns, which is done without inverting  $g$ , which is why Lagrange multipliers can be so useful.

For multiple constraints  $g_1 = 0, g_2 = 0, \dots$ ,

$$\nabla f + \lambda_1 \nabla g_1 + \lambda_2 \nabla g_2 + \dots = 0.$$

This method is helpful because it converts a constrained optimization problem into a system of equations without constraints by introducing additional variables called Lagrange multipliers [6, 7, 8, 9]. The advantage of using Lagrange multipliers is their ability to operate complex constraints efficiently, allowing the solution of high-dimensional problems. Sometimes, in other computational approaches, these optimization approaches are computationally intensive and impractical to solve using direct substitution methods. In this method, by equating the gradients of the objective function and the constraints, Lagrange multipliers provide critical insight into the essence of the solutions by pointing to the linear relationship of the gradients and, as a consequence, identifying possible maxima within the specified constraints. This technique is essential in many fields, such as engineering, physics, and economics, where it is mandatory to optimize the real application under constraints frequently.

The Lagrange Multiplier model is appreciated for its computational simplicity and efficiency, especially when alternative models are complex and their computationally demanding estimation [18]. In thermodynamics, the Lagrange Multiplier method is utilized mainly to use the entropy principle effectively. This principle evaluates the limitations on the fundamental relationships of materials or alloys to ensure that inequalities are maintained throughout all thermodynamic processes. The method simplifies this process by incorporating field equations and their linear combinations with entropy inequalities, where the coefficients of these combinations act as Lagrange multipliers. This approach transforms the complex problem of satisfying the entropy inequality into a more manageable algebraic form, making it easier to derive necessary restrictions for the constitutive equations of various materials. This method is particularly advantageous because it facilitates the derivation process by reducing the computational complexity [19]. Given the above considerations, we applied Lagrange multipliers in our theoretical model, subject to thermodynamic constraints.

## 2 CALPHAD

CALPHAD, Calculation of Phase Diagrams, is an essential tool in materials science that leverages thermodynamics to predict phase stability and material behavior across a range of conditions.[20, 21] The history of CALPHAD manifests the progress likely in phase equilibria by leveraging fundamental thermodynamic principles alongside mathematical modeling to illuminate the diverse thermodynamic characteristics of phases. This approach, CALPHAD, demonstrates the continual enhancements made to a complex and scholarly field, showing its practical applicability and broad scope of use. The origins of the CALPHAD methodology are traced back to van Laar in 1908, who utilized Gibbs energy formulations to study phase equilibria at the dawn of the 20th century.[22]

The CALPHAD method uses a thermodynamic framework to predict phase stability and transformations in various materials under different conditions. It focuses on minimizing Gibbs free energy, with each phase's energy modeled as a temperature, composition, and pressure function. A vital aspect of CALPHAD is the development of extensive thermodynamic databases that combine experimental data and theoretical calculations for more reasonable precision. This iterative refinement of databases and modeling techniques makes CALPHAD a valuable tool in materials science, enabling precise material design and complex material behaviors before exploratory verification.[20, 21]

By minimizing the Gibbs energy, CALPHAD provides insights into both stable and metastable equilibria, with broad implications in alloy design, process optimization, thermodynamic database development, diffusion modeling, etc. It enables the design of new alloys by forecasting phase formations under specific conditions such as temperature, composition, and pressure. This predictive capability is critical for engineering materials with targeted mechanical properties and enhanced corrosion resistance. CALPHAD facilitates a deep understanding of how various manufacturing processes, particularly heat treatments, influence material microstructures, allowing fine-tuning processing parameters to reach optimal performance. [20]

The methodology predicts material responses to environmental exposures, which is invaluable for assessing corrosion, degradation, and long-term stability. CALPHAD extends its predictive power to model microsegregation and the emergence of non-equilibrium phases in processes like rapid cooling or welding, where equilibrium assumptions break down. This capability fills a critical gap left by conventional equilibrium phase diagrams. A corner-

stone of CALPHAD is the continuous refinement of thermodynamic databases. These holds of experimental and calculated data ensure that predictions remain accurate and relevant as new information becomes available. Beyond phase predictions, CALPHAD integrates diffusion simulations by calculating diffusion coefficients. This is crucial for understanding and predicting material behavior during thermal treatments and other diffusion-controlled processes. [21]

Fundamentally, CALPHAD is a groundbreaking approach in the materials fields, enabling the simulation and optimization of materials and processes prior to physical investigation. This predictive advantage preserves valuable resources and time and drives innovation in material design and manufacturing.

### 3 Motivation

Intrinsic stress is ubiquitous in crystalline solids and is essential to understanding their microstructures and properties. Independent from external loading, intrinsic stress arises from defects in the crystalline structure, such as dislocations or interfaces. Coherency stress is commonly present in critical classes of materials such as superalloys, steels, and semiconductors. Coherency stress arises from lattice misfit between phases that can maintain the continuity of the crystal structure across their interface. Lattice misfits below a threshold for a given pair of phases can be accommodated purely by elastic strain. The elastic strain energy associated with the lattice misfit contributes to the total energies of the phases and thus may affect phase equilibria and their graphical representation in phase diagrams.

Since the publication of the pioneering work by Larché and Cahn [23], the impact of stress on thermodynamics of alloys have been of sustained interest [24, 25, 26]. Significant progress has been made in capturing coherency stress effects specifically and calculating coherency phase diagrams. Cahn and Larché [23] developed a simple model for binary infinitely-sized solids consisting of two phases with identical isotropic elastic properties but different lattice parameters. Their analysis demonstrated that coherency strains stabilize a single-phase system relative to a two-phase one. Further investigations of the differences in thermodynamics of stressed solids and stress-free fluid-like systems [27, 28] can be summarized as follows: (i) tie lines and field lines can deviate, (ii) multiple linearly stable equilibrium states can exist under identical thermodynamic conditions, (iii) the common

tangent construction does not apply, and (iv) the Gibbs phase rule no longer holds, i.e., the number of phases in equilibrium is independent of thermodynamic degrees of freedom. The precise thermodynamic boundaries where classical and coherent phase representations converge remain an open question, warranting further investigation. Johnson and Voorhees [15] assessed the Cahn's model and outlines some consequences of coherency strains and long-range elastic stress on the thermodynamic equilibrium of coherent solids. However, they didn't construct a phase diagram and determine the boundaries for interpreting the equilibrium phase composition and volume fraction. Recent studies generalized the Cahn-Larché model from an idealized to more realistic systems by capturing the effects of: a free surface [29], a large lattice mismatch [30], anisotropy [31]. Beyond theoretical formulations building on the Cahn-Larché model, thermodynamics and phase diagrams of coherent systems have been pursued with computational methods. Wood and Zunger introduced a first-principles approach to calculating coherent phase diagrams using the density functional theory and cluster variation method [32]. They investigate the impact of epitaxial growth on the phase diagrams and thermodynamic properties of binary or pseudobinary alloys through a cluster-based theoretical framework. It mainly studies how thin films grown on substrates influence these properties, presenting phenomena such as 'Epitaxial Stabilization', where ordered phases absent in bulk can emerge under epitaxial conditions and disordered phases remain stable at lower temperatures. The study uses continuum elasticity and microscopic cluster theories to reveal how epitaxial constraints modify alloy behaviors due to strain and lattice-matching effects, which are essential for semiconductor and metal alloy growth [32]. Stress effects have also been of continued interest in the phase field community, inquiring about the impact of coherent stress on the microstructure evolution in materials, ranging from the classical works of Khachaturyan [33] to recent developments of chemomechanics phase field methods from isotropic to anisotropic interface by introducing anisotropic expression of the elastic energy. This approach overcomes the limit of Cahn's model, which fails to predict accurately the evolution of phase equilibria for large deformation. Garcke and Weikard [34] discussed the kinetic aspect of phase separation in binary alloy using the Cahn-Hilliard equation. By applying finite element approximation, they showed the impact of elasticity on the morphology of the microstructure. The coherency strain accommodation alters both thermodynamics and kinetics of the phase transformations, so that are considered in phase field research [35, 36]. This large body of published work mostly focused on

systems in solid state. With few exceptions [37, 38, 39], the effect of stress on equilibria in multiphase systems that include a liquid phase has not been investigated in detail. In this theoretical study, we model the effect of coherency stress on invariant points of phase diagrams including a liquid. Accurate modeling of eutectic and peritectic points in alloys is important for understanding and predicting microstructure formation during processing, computational design of alloys, and their inoculants, favorable for metal additive manufacturing. Given this importance, we leverage the original Larche-Cahn formulation to evaluate the effects of coherency stress on eutectic and peritectic points in binary alloys that form two coherent solid phases.

## 4 Theoretical model

In our study, we used a computational method to predict the thermodynamic equilibrium of coherent binary alloys. Our model imitates various levels of coherent stress to evaluate the conditions under which the solid phases,  $\alpha$  and  $\beta$ , and a liquid phase,  $L$ , can exist in equilibrium. This method thoroughly evaluates how stable each phase is under conditions described by our computational model.

Our study considers binary alloy systems consisting of two elements  $A$  and  $B$ . These systems form solid phases at low temperatures:  $A$ -rich  $\alpha$  phase and  $B$ -rich  $\beta$  phase with limited solubility of the other element. The system can form an invariant point in which both phases are in equilibrium with a liquid phase,  $L$ . Our goal is to construct a theoretical model that will provide conditions for such three-phase equilibrium in the presence of a coherency stress between the solid phases. To facilitate an analytical solution, we use simplifying assumptions about the system similar to those used in the original Larché-Cahn model for two-phase systems [23]. Specifically, we consider an infinite volume occupied by three phases; the solid phases are isotropic and linearly elastic; both solid phases have the same elastic properties described by, e.g., Young’s modulus  $E$  and Poisson’s ratio  $\nu$ . These simplifying assumptions allow the coherency energy,  $g_e$ , to depend only on the molar fractions of the solid phases ( $z_\alpha$  and  $z_\beta$ ) and the elastic energy associated with the lattice misfit,  $\epsilon$ :

$$g_e = z_\alpha z_\beta \frac{VE\epsilon^2}{(1-\nu)} = z_\alpha z_\beta \mathcal{W}, \quad (5)$$

where we introduce the notation  $\mathcal{W} = VE\epsilon^2/(1-\nu)$ . The coherency energy contribution,  $g_e$  is additive to the chemical energies of the phases represented by molar Gibbs free energies,  $g_i$  (with  $i \in \{\alpha, \beta, L\}$ ) that constitute the total molar energy of the system,  $g$ :

$$g(z_\alpha, z_\beta, x_\alpha, x_\beta, x_L) = z_L g_L(x_L) + z_\alpha g_\alpha(x_\alpha) + z_\beta g_\beta(x_\beta) + z_\alpha z_\beta \mathcal{W} \quad (6)$$

where  $x_i$  is the composition of the  $i$ th phase expressed as a concentration of element  $B$ :  $x_i = N_i^B/(N_i^A + N_i^B)$  with  $N_i^A$  and  $N_i^B$  representing the number of moles of elements  $A$  and  $B$  in the  $i$ th phase. For an alloy of the overall composition,  $X$ , the phase molar fractions and compositions must satisfy the mass balance and the ranges given their definitions:

$$X = (1 - z_\alpha - z_\beta)x_L + z_\alpha x_\alpha + z_\beta x_\beta \quad (7a)$$

$$z_\alpha + z_\beta + z_L = 1 \quad (7b)$$

$$0 \leq z_\alpha, z_\beta, z_L, x_\alpha, x_\beta, x_L, X \leq 1 \quad (7c)$$

Here,  $X$  is also expressed as a total molar concentration of  $B$ :  $X = N^B/(N^A + N^B)$  with  $N^A$  and  $N^B$  denoting the total moles of  $A$  and  $B$  elements in the alloy.

Minimizing the total Gibbs free energy in Equation (6) subject to the constraints in Equation (7) leads to the conditions for equilibrium in terms of  $z$  and  $x$  values. The global minimum can be found using the method of Lagrange multipliers. To this end, we introduce a Lagrangian:

$$\begin{aligned} \mathcal{L} = & z_L g(x_L) + z_\alpha g(x_\alpha) + z_\beta g(x_\beta) + \mathcal{W} z_\alpha z_\beta \\ & - \lambda(z_L x_L + z_\alpha x_\alpha + z_\beta x_\beta - X), \end{aligned} \quad (8)$$

where  $\lambda$  is a Lagrange multiplier. Requiring partial derivatives of the Lagrangian in respect to the seven independent variables ( $z_\alpha, z_\beta, z_L, x_\alpha, x_\beta, x_L, \lambda$ ) be equal to zero allows us to find the sought minimum of the Gibbs free energy from the following equations:

$$\frac{\partial \mathcal{L}}{\partial x_\alpha} = -g_L(x_\alpha) + g_\alpha(x_\beta) + \mathcal{W}z_\beta - \lambda(-x_L + x_\alpha) = 0 \quad (9a)$$

$$\frac{\partial \mathcal{L}}{\partial x_\beta} = -g_L(x_L) + g_\beta(x_\beta) + \mathcal{W}z_\alpha - \lambda(-x_L + x_\beta) = 0 \quad (9b)$$

$$\frac{\partial \mathcal{L}}{\partial x_L} = (1 - z_\alpha - z_\beta)\left(\frac{dg_L}{dx_L} - \lambda\right) = 0 \quad (9c)$$

$$\frac{\partial \mathcal{L}}{\partial x_\alpha} = z_\alpha\left(\frac{dg_\alpha}{dx_\alpha} - \lambda\right) = 0 \quad (9d)$$

$$\frac{\partial \mathcal{L}}{\partial x_\beta} = z_\beta\left(\frac{dg_\beta}{dx_\beta} - \lambda\right) = 0 \quad (9e)$$

$$\frac{\partial \mathcal{L}}{\partial \lambda} = (1 - z_\alpha - z_\beta)x_L + z_\alpha x_\alpha + z_\beta x_\beta - X = 0 \quad (9f)$$

Rearranging these six equations that set the partials equal to zero, where  $0 < z_\alpha, z_\beta, z_\alpha + z_\beta < 1$ , provides the following equations (i.e., solution with non-zero molar fractions of the phases):

$$\frac{dg_L}{dx_L} = \frac{dg_\alpha}{dx_\alpha} = \frac{dg_\beta}{dx_\beta} = \frac{g_\alpha(x_\alpha) - g_L(x_L) + \mathcal{W}z_\beta}{x_\alpha - x_L} = \frac{g_\beta(x_\beta) - g_L(x_L) + \mathcal{W}z_\alpha}{x_\beta - x_L} \quad (10)$$

In general there are seven possible solutions as follows:

$$\text{Minimum} : g_L(X), \text{ when } z_\alpha \text{ and } z_\beta = 0 \quad (11a)$$

$$\text{Minimum} : g_\alpha(X), \text{ when } z_L \text{ and } z_\beta = 0 \quad (11b)$$

$$\text{Minimum} : g_\beta(X), \text{ when } z_L \text{ and } z_\alpha = 0 \quad (11c)$$

When the  $\beta$ - $L$  two-phase region is thermodynamically more stable, the Gibbs energy of this mixture of phases is lower than that of any other phases. The  $\alpha$  phase does not appear in the equilibrium phase region, and its molar fraction is zero.

$$(1 - z_\beta)g_L(x_L) + z_\beta g_\beta(x_\beta), \text{ where } z_\alpha = 0$$

Where,  $z_\beta, x_\beta, x_L$  are found by the equations,

$$\frac{dg_L}{dx_L} = \frac{dg_\beta}{dx_\beta} = \frac{g_\beta(x_\beta) - g_L(x_L)}{x_\beta - x_L}, z_\beta = \frac{X - x_L}{x_\beta - x_L} \quad (12)$$

When the  $\alpha$ - $L$  two-phase region is thermodynamically more stable, the Gibbs energy of this mixture of phases is lower than that of any other phases. The  $\beta$  phase does not appear in the equilibrium phase region, and its molar fraction is zero.

$$(1 - z_\alpha)g_L(x_L) + x_\alpha g_\alpha(x_\alpha), \text{ where } z_\beta = 0$$

Where,  $z_\alpha, x_\alpha, x_L$  are found by the equations,

$$\frac{dg_L}{dx_L} = \frac{dg_\alpha}{dx_\alpha} = \frac{g_\alpha(x_\alpha) - g_L(x_L)}{x_\alpha - x_L}, z_\alpha = \frac{X - x_L}{x_\alpha - x_L} \quad (13)$$

When two solid phases,  $\alpha$ - $\beta$  are present and there is no liquid,  $L$  phase,

$$z_\alpha g_\alpha(x_\alpha) + x_\beta g_\beta(x_\beta) + \mathcal{W}z_\alpha z_\beta, \text{ where } z_L = 0$$

Where,  $z_\alpha, z_\beta, x_\alpha, x_\beta$  are found by the following equations,

$$\frac{dg_\alpha}{dx_\alpha} = \frac{dg_\beta}{dx_\beta} = \frac{g_\alpha(x_\alpha) - g_\beta(x_\beta) + \mathcal{W}(1 - 2z_\alpha)}{x_\alpha - x_\beta}, z_\alpha = \frac{X - x_\beta}{x_\alpha - x_\beta} \quad (14)$$

When there are three phases,  $\alpha$ - $\beta$ - $L$  coexist,

$$(1 - z_\alpha - z_\beta)g_L(x_L) + z_\alpha g_\alpha(x_\alpha) + z_\beta g_\beta(x_\beta) + \mathcal{W}z_\alpha z_\beta$$

Where  $z^\alpha, z^\beta, x^L, x^\alpha, x^\beta$  are found by,

$$\frac{dg_L}{dx_L} = \frac{dg_\alpha}{dx_\alpha} = \frac{dg_\beta}{dx_\beta} = \frac{g_\alpha(x_\alpha) - g_L(x_L) + \mathcal{W}z_\beta}{x_\alpha - x_L} = \frac{g_\beta(x_\beta) - g_L(x_L) + \mathcal{W}z_\alpha}{x_\beta - x_L} \quad (15a)$$

$$X = (1 - z_\alpha - z_\beta)x_L + z_\alpha x_\alpha + z_\beta x_\beta \quad (15b)$$

$$z_\alpha = \frac{X - x_L}{x_\alpha - x_L} + z_\beta \left( \frac{x_L - x_\beta}{x_\alpha - x_\beta} \right) \quad (15c)$$

Solving these equations for a specific set of functions describing the Gibbs free energies of individual phases (e.g., from thermodynamic databases) provides conditions for thermodynamic equilibrium of the three phases. Note that, setting the coherency term to zero,  $\mathcal{W} = 0$ , in Equation (10), we recover classical equations that graphically represent the well-known common-tangent construction. The classical common-tangent rules follow from Equation (16) for two-phase equilibria between the liquid and either of the solid phases because the additional coherency terms diminish when  $z_\alpha = 0$  or  $z_\beta = 0$ .

$$\frac{dg_L}{dx_L} = \frac{dg_\alpha}{dx_\alpha} = \frac{dg_\beta}{dx_\beta} = \frac{g_\alpha(x_\alpha) - g_L(x_L)}{x_\alpha - x_L} = \frac{g_\beta(x_\beta) - g_L(x_L)}{x_\beta - x_L} \quad (16)$$

With the non-zero coherency stress,  $\mathcal{W} \neq 0$  and, in the presence of both solid phases, the common tangent construction does not hold for the coherent solid phases. Instead, the equilibrium between two solid phases is graphically represented by concave curves whose curvature depends on the magnitude of the coherency stress, consistent with the results of

Cahn and Larche [23]. Solving the equations in Equation (10) with  $\mathcal{W} \neq 0$  for combinations of different temperatures and alloy compositions,  $(X, T)$  allows us to obtain phase equilibria in maps reminiscent of phase diagrams. We refer to them as *phase equilibria maps* because they display phases in equilibrium-like phase diagrams that possess features of classical phase diagrams, such as the lever rule.

## 5 Case studies

### 5.1 General approach and specific functional forms of Gibbs free energies

We present two case studies that use the general theoretical model presented in the previous section to elucidate the impact of coherency stress on invariant points. The two case studies consider (i) a eutectic-forming binary alloy system and (ii) a binary system with a peritectic. To focus on the fundamental and qualitative effects of the coherency stress, we consider simple quadratic functions to describe the molar Gibbs free energies of the solid phases:

$$g_\alpha = a(x_\alpha - x_\alpha^0)^2 + b_\alpha \quad (17a)$$

$$g_\beta = a(x_\beta - x_\beta^0)^2 + b_\beta \quad (17b)$$

parametrized by unique sets of scalar  $x^0$ ,  $a$ ,  $b$  parameters. We use a similar functional form for the liquid phase with the addition of a linear dependence on temperature,  $T$ :

$$g_L = a(x_L - x_L^0)^2 + b_L - T \quad (18)$$

Our selected parametrization of the Gibbs free energy functions (Equations (17) and (18)) allows us to investigate both eutectic- and peritectic-forming binary systems by suitable selection of the  $x^0$  parameters that control the position of the parabolic curves. A eutectic point can be introduced by setting  $x_\alpha^0 < x_L^0 < x_\beta^0$ , whereas  $x_L^0 < x_\alpha^0 < x_\beta^0$  represents a system with a peritectic point. Since the specific curvature of the Gibbs free energy curves does not affect the results sought in this study, the  $a$  parameter controlling the shape is adopted identical for all three  $g$  functions. In terms of specific values, we choose such a combination of parameter values that ensures that the eutectic and peritectic points fall within the selected temperature range. Our parameter selection represents binary systems

where the melting points of the solid phases are comparable and are both much higher than the invariant points.

These functional forms and parameter selections, albeit simple, allow us to elucidate the fundamental effects of coherency stress on three-phase equilibria at invariant points. To this end, we substitute these Gibbs free energy functions (Equations (17) and (18)) into Equation (10) and solve the resulting system of equations for a given combination of alloy composition,  $X$ , temperature,  $T$ , and coherency term,  $\mathcal{W}$ . Solving the equations provides us with molar fractions,  $z_i$ , and concentrations  $x_i$  (e.g., of element  $B$ ) of the phases in equilibrium under given conditions. Obtaining phase molar fractions for systematically varied alloy compositions,  $X$ , and temperatures,  $T$ , allows us to construct phase equilibria maps to visualize the impact of coherency stress on eutectic and peritectic regions of binary phase diagrams.

## 5.2 Computer implementation

We developed the following algorithm, implemented in Python, to streamline the solution of the systems of equations for many combinations of  $(X, T)$  required for the construction of phase equilibria maps.

1. Solve equations for pairwise two-phase equilibria in solid phases and the liquid ( $\alpha$ - $L$ ,  $\beta$ - $L$ )
2. Solve equations for two-phase equilibria including the two solid phases ( $\alpha$ - $\beta$ )
3. Solve equations for three-phase equilibria including all three phases ( $\alpha$ - $\beta$ - $L$ ).
4. Calculate the Gibbs free energies corresponding to seven potential cases of equilibrium: three single-phase, three two-phase, and one three-phase conditions.
5. For each overall alloy composition,  $X$ , and temperature,  $T$ , find the equilibrium that corresponds to the lowest Gibbs free energy and store the corresponding label that lists phases with non-zero molar fractions.
6. Visualize the results as fields of labels that list the phases in equilibrium.

Our implementation leverages the library `sympy` for the symbolic solution of systems of equations in Python. The next subsections demonstrate the application of this approach and its computer implementation to simple eutectic and peritectic systems.

### 5.3 Case study 1: Eutectic system

We first consider the application of our theoretical model (Section 4) for a binary system that includes a eutectic point in its conventional, stress-free phase diagram. To this end, we set  $x_\alpha^0 < x_L^0 < x_\beta^0$  in our functions describing the Gibbs free energies of the phases (Equations (17) and (18)). Table 3 lists a specific set of values we adopted for all the parameters in the Gibbs free energy functions. We then analyze the Gibbs free energy curves corresponding to equilibria of different combinations of the phases (Figure 7) and phase equilibria maps for a full range of overall compositions,  $X \in [0, 1]$ , and a temperature range that includes the eutectic point or field.

Table 3: Parameters for Eutectic system for the Gibbs energy function

Parameter name	Parameter Values
$x_\alpha^0$	0.2
$x_\beta^0$	0.8
$x_L^0$	0.5
a	50
$b_\alpha$	20
$b_\beta$	20
$b_L$	30

Figure 7 shows the impact of the coherency term on Gibbs free energy curves of phase combinations at three temperatures: (i) below, (ii) equal to, and (iii) above the eutectic temperature,  $T_E$ , in the stress-free phase diagram. In the absence of the coherency stress,  $\mathcal{W} = 0$ , our calculations reproduce the traditional common-tangent construction. At  $T > T_E$ , the common tangent between  $g^\alpha$  and  $g^\beta$  curves indicates equilibrium between the  $\alpha$  and  $\beta$  phases.

Our findings concerning the strain effects on the eutectic equilibrium included: (i) in the presence of coherency strain energy, the three-phase equilibrium at the original eutectic temperature,  $T_E$ , is thermodynamically unfavorable; and (ii) below  $T_E$ , three-phase equilibrium is stabilized by relatively moderate strain energy. Below  $T_E$  (e.g., at  $T_1$  in Figure 7) and with low coherency energy, a mixture of two solid phases ( $\alpha$  and  $\beta$ ) is more stable than the liquid as in the strain-free case (Figure 7 (a)). Three phases ( $\alpha$ - $\beta$ - $L$ ) are in equilibrium

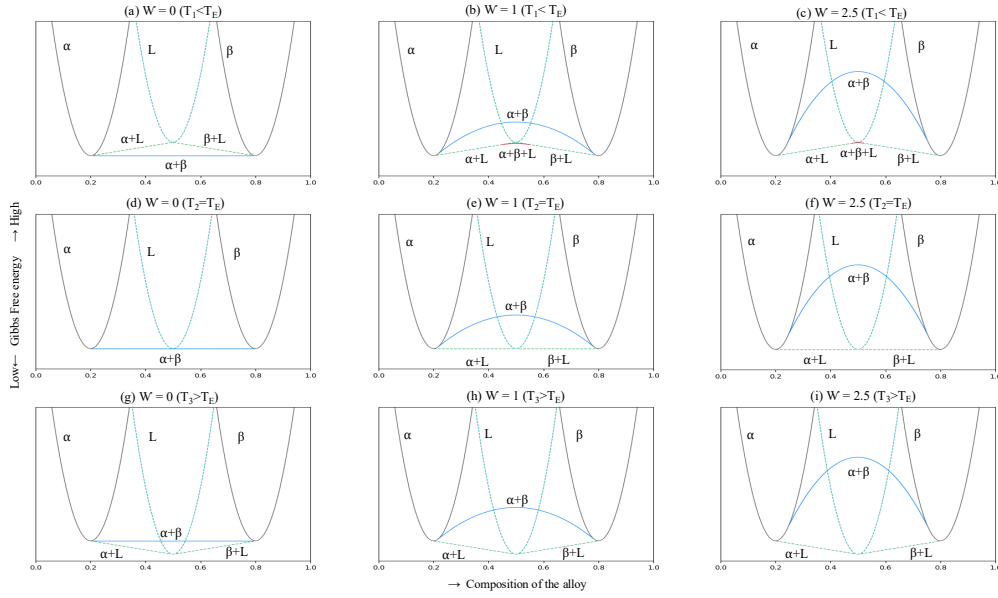


Figure 7: Gibbs free energy curve under different coherency stress for Eutectic Binary-phase equilibria for below, at, and above Eutectic temperature ( $T_E$ )

at moderate elastic energies for a range of alloy compositions (red shaded in Figure 7. This range becomes narrow with an increase in the strain energy and completely disappears after a threshold value, which makes solid+liquid mixtures ( $\alpha$ -L or  $\beta$ -L) more thermodynamically favorable (straight lines in Figure 7 (c)). Figure 8 presents a magnified projection of Figure 7 (c) where the three-phase ( $\alpha$ - $\beta$ -L) region is bounded by the red-shaded line under coherency stress level 2.5. Here, the two solid-phase regions ( $\alpha$ - $\beta$ ) deviate more from the common tangent characteristics, making the solid-liquid phase regions ( $\alpha$ -L and  $\beta$ -L) more stable and forming the three-phase region.

In our model, we minimize the energy of the phases within a range of temperatures and compositions and obtain the composition corresponding to the equilibrium state by applying the Lagrange multipliers method, as previously described. We consider minimizing the value of the Gibbs free energy of the  $\alpha$ ,  $\beta$ , and  $L$  phases, and this minimization leads to the establishment of common tangent constructions representing mixtures of the phases. The three-phase equilibrium, or the eutectic point, occurs at the eutectic temperature ( $T_E$ ). At this point, represented as  $\alpha$ - $\beta$ -L, the system theoretically converges to a singular point. As the temperature varies around  $T_E$ , significant changes are observed in the Gibbs energy

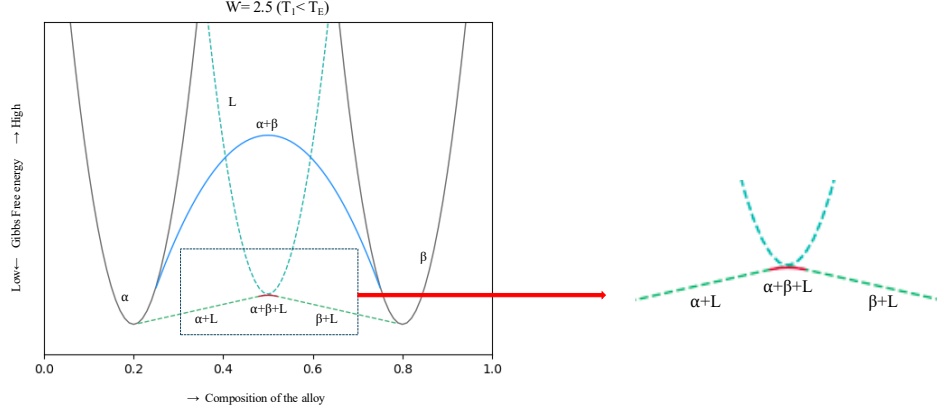


Figure 8: Magnified projection of Gibbs energy curves for the three-phase region ( $\alpha$ - $\beta$ - $L$ ) curve under coherency stress level 2.5.

profiles for the phases, particularly the liquid phase. At higher temperatures ( $T > T_E$ ), the Gibbs energy of the liquid phase becomes lower than that of the other two solid phases, resulting in a more stable liquid phase. The common tangent between the phases of  $\alpha$  and  $\beta$  deviates from its known characteristics. It forms a concave curve upward for both cases  $T$  above and below  $T_E$  as shown in Figure 7 due to the presence of coherency stress between these two solid phases. The higher the level of the coherency stress, the more upward the  $\alpha$ - $\beta$  concave curve becomes, and the more unstable the  $\alpha$ - $\beta$  area becomes. This upward shift and corresponding instability are directly proportional to the level of coherency stress present.

When the level of coherency stress,  $\mathcal{W} = 0$ , the eutectic condition is only one invariant point with zero degrees of freedom, following Eq. 10, as shown in Figure 9 (a). However, the formation of the  $\alpha$ - $\beta$ - $L$  is observable as the coherency stress  $\mathcal{W}$  increases. This occurs because the conditions of the Gibbs phase rule are violated with the rise in coherency stress, as discussed in the Section 4. Therefore, the three-phase region,  $\alpha$ - $\beta$ - $L$  is not a single point, as shown in Figure 9 (a), but rather an area in the phase map as shown in Figure 9 (b), (c), (d), (e) and (f). The increase of the  $\mathcal{W}$  results in increasing the three-phase region,

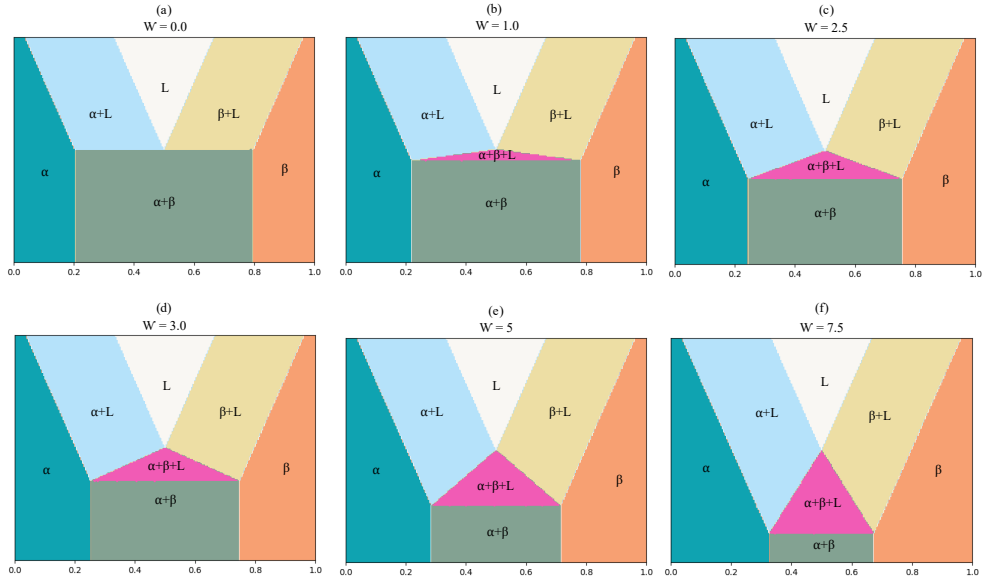


Figure 9: Eutectic Binary-phase equilibrium map under different coherency stresses

$\alpha$ - $\beta$ - $L$  invading downward, occupying the  $\alpha$ - $\beta$  region, thus narrowing the width of the  $\alpha$ - $\beta$  region.

#### 5.4 Case study 2: Peritectic system

Now, we consider the application of our theoretical model (Section 4) for the binary system that includes a peritectic point in its conventional, stress-free phase diagram. To this end, we set  $x_L^0 < x_\alpha^0 < x_\beta^0$  in our functions describing the Gibbs free energies of the phases (Equations (17) and (18)). Same as for the eutectic case, Table 4 lists a specific set of values we adopted for all the parameters in the Gibbs free energy functions for our peritectic system. By analyzing the Gibbs free energy curves corresponding to equilibria of different combinations of the phases (Figure 10), we get the phase equilibria maps (Figure 11) for a full range of overall compositions,  $X \in [0, 1]$ , and a temperature range that includes the peritectic point or field. From the Gibbs energy functions of the three phases for the eutectic system, by setting  $x_L^0 < x_\alpha^0 < x_\beta^0$  instead of  $x_\alpha^0 < x_L^0 < x_\beta^0$ , we obtain our peritectic phase equilibria maps, keeping all other conditions identical.

Similar to the eutectic case study, in the peritectic case study, we consider the  $L$  phase only as temperature-dependent, and as before, we minimize the Gibbs energy of the phases

Table 4: Parameters for Peritectic system for the Gibbs energy function

Parameter name	Parameter Values
$x_{\alpha}^0$	0.5
$x_{\beta}^0$	0.8
$x_L^0$	0.3
a	50
$b_{\alpha}$	21
$b_{\beta}$	21
$b_L$	40

within a range of temperatures and compositions and obtain the composition corresponding to the equilibrium state by applying Lagrange multipliers. We consider the minimized value of the Gibbs free energy considering Equations (17) and (18). Here, we consider the parameter  $b$  as 21 for the two solid phases compared to the eutectic case. We select this parameter value to get a peritectic point within a temperature range, as the parameter  $b$  sets the function's minimum height as the minimum Gibbs energy for the solid phases (Equation (17)). If we consider the parameter  $b_{\alpha}$  and  $b_{\beta}$  to be identical to that of the eutectic system, the peritectic point will form at a higher temperature. This is because the temperature-dependent Gibbs energy function for the liquid (as described by Equation (18)) reaches its minimum when in equilibrium with the two solid phases. Consequently, the invariant peritectic point occurs at a higher temperature due to the smaller parameter values of  $b_{\alpha}$  and  $b_{\beta}$  associated with the solid phases. There are no bounds for selecting these parameters; we choose them to achieve a peritectic point within a standard temperature range.

Figure 10 shows the impact of the coherency term on Gibbs free energy curves of phase combinations at three temperatures: (i) below, (ii) equal to, and (iii) above the peritectic temperature,  $T_P$ , in the stress-free phase diagram. In the absence of the coherency stress,  $\mathcal{W} = 0$ , our calculations reproduce the traditional common-tangent construction same as the eutectic system. At  $T > T_P$ , the common tangent between  $g^{\alpha}$  and  $g^{\beta}$  curves indicates equilibrium between  $\alpha$  and  $\beta$  phases as the  $\mathcal{W} = 0$  is not able to violate the common tangent rule. Moreover, our findings for the peritectic equilibrium considering the strain

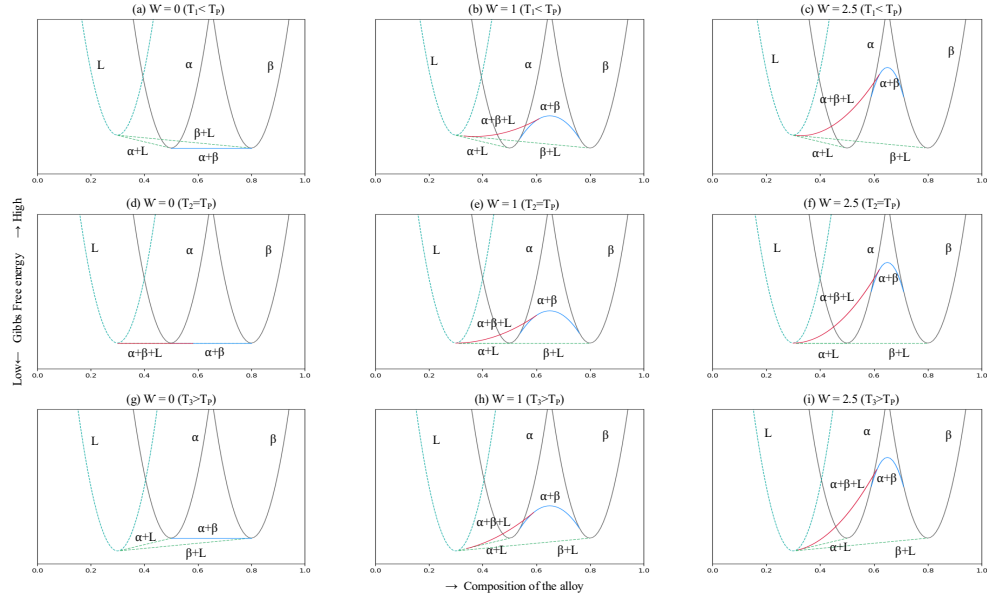


Figure 10: Gibbs free energy curve under different coherency stress for Peritectic Binary-phase equilibria for below, at, and above Peritectic temperature ( $T_P$ )

effects, included: (i) in the presence of coherency strain energy, the three-phase equilibrium at the original peritectic temperature,  $T_P$ , is thermodynamically unfavorable; and (ii) below  $T_P$ , three-phase equilibrium is still thermodynamically unfavorable by relatively moderate strain energy. Below  $T_P$  (e.g., at  $T_1$  in Figure 10) and with low coherency energy, a mixture of two solid phases ( $\alpha$  and  $\beta$ ) is more stable than the liquid phase as in the strain-free case Figure 10 (a). Three phases ( $\alpha$ - $\beta$ - $L$ ) are in equilibrium at moderate elastic energies for a range of alloy compositions (shaded in red Figure 10), still unfavourable than the mixture of one solid and liquid phases ( $\alpha$ - $L$  and  $\beta$ - $L$ ). However, this range becomes wide with an increase in the strain energy (shaded in red Figure 10) and the mixture of two solid phases ( $\alpha$ - $\beta$ ) completely disappears after a threshold value, which makes solid and liquid mixtures ( $\alpha$ - $L$  or  $\beta$ - $L$ ) more thermodynamically favorable (straight lines in Figure 10 (c), (f), (i)).

In this binary system, the three-phase equilibrium at the peritectic point ( $\alpha$ - $\beta$ - $L$ ) occurs at a specific arbitrary temperature and composition with zero degree of freedom. At this temperature, one solid,  $\beta$ , and one liquid,  $L$ , phase combine to form a second, distinct solid phase,  $\alpha$ , as shown in Figure 11 (a). This transformation occurs under conditions without

coherency stress ( $\mathcal{W}=0$ ) between the solids.

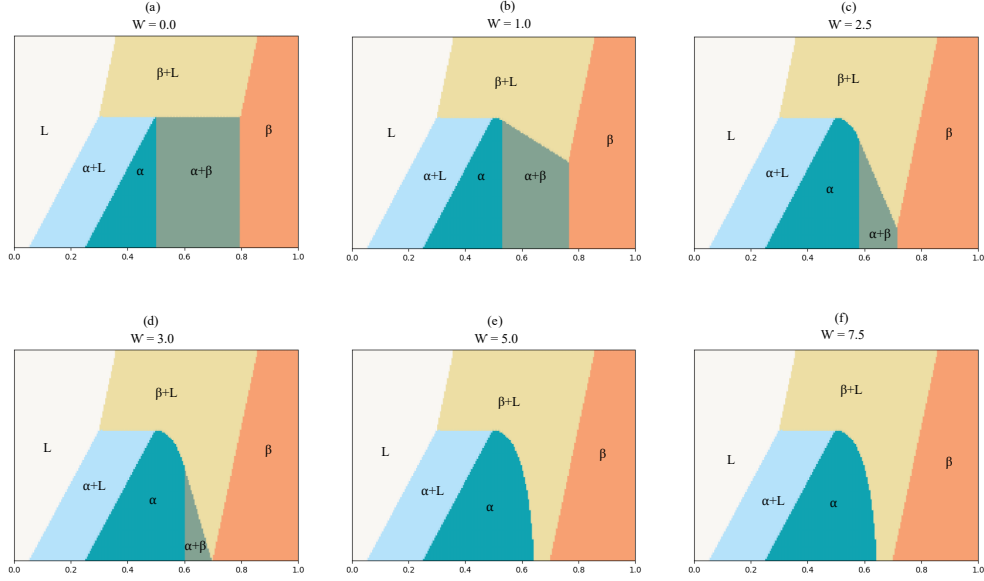


Figure 11: Peritectic Binary-phase equilibrium map under different coherency stresses

With the increase of the coherency stress in the system, the peritectic phase diagram shows unique characteristics because of the melting point of the two elements  $A$  and  $B$  as in their solid phases that are not similar to those of the eutectic one, which is a significant motivation to study the peritectic phase diagram. In an eutectic phase diagram, the melting points of the two elements are almost identical, contrasting with the peritectic diagram. In the peritectic phase diagram, the peritectic point is above the melting point of element  $A$ , which primarily forms the  $\alpha$  phase. In contrast, the melting point of element  $B$ , which primarily forms the  $\beta$  phase, is higher than the temperature of the peritectic point. As coherency stress between the solids increases, the  $\alpha$ ,  $\beta$ , and  $L$  phases initially combine. However, this combination does not form a three-phase region, which is comparatively more unstable than the other regions due to differences in the melting temperatures of the elements  $A$  and  $B$ . At increasing coherency stress between the solids, the  $\beta$ - $L$  region is more stable than the  $\alpha$ - $\beta$ - $L$  region, primarily because the  $\alpha$  phase, which is solid  $A$  has a lower melting point. When the coherency stress  $\mathcal{W}$  is considered to be one unit, the  $\beta$ - $L$  region increases, while the coexistence of the two solid phases, the  $\alpha$ - $\beta$  region, decreases. Furthermore, after a certain level of coherency stress, the total Gibbs free energy of the  $\alpha$  and  $\beta$  phase

significantly increases with the higher coherency stress level. This rise in free energy yields the combination of  $\alpha$ - $\beta$  region to become unstable, resulting in its disappearance, as depicted in Figure 11 (e) and (f).

## 5.5 Application of lever-rule on phase equilibria map

At first glance, significant coherency stress suggests that the conventional lever rule may not strictly apply within the  $\beta$ - $L$  two-phase region in the peritectic case study. Specifically, if a tie-line is drawn through the  $\beta$ - $L$  region below the peritectic temperature, it appears to connect the  $\beta$  phase boundary on one side and the  $\alpha$  phase boundary on the other, indicating a deviation from the expected  $\beta$ - $L$  equilibrium. However, if we look at the Gibbs free energy curves in Figure 10 (c) for the peritectic one, we notice that the  $\beta$ - $L$  phase exists; thus, the phase fractions of the  $\beta$  and  $L$  phases within the  $\beta$ - $L$  region can be determined accordingly.

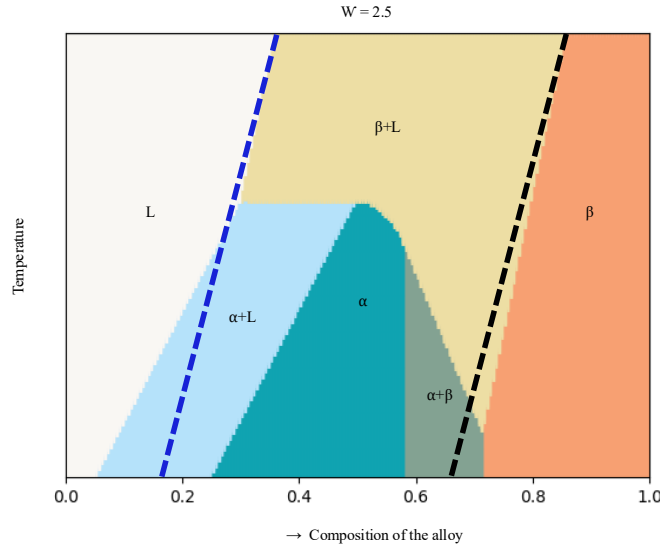


Figure 12: Calculated  $\beta$ - $L$  Phase Boundaries (blue dashed line:  $L$  phase boundary, black dashed line:  $\beta$  phase boundary)

Figure 12 shows the calculated  $\beta$ - $L$  phase boundaries within the phase equilibria map in our model for the peritectic case, where the blue dashed line corresponds to the liquidus boundary, representing the composition of the liquid phase ( $x_L$ ) at each temperature, while

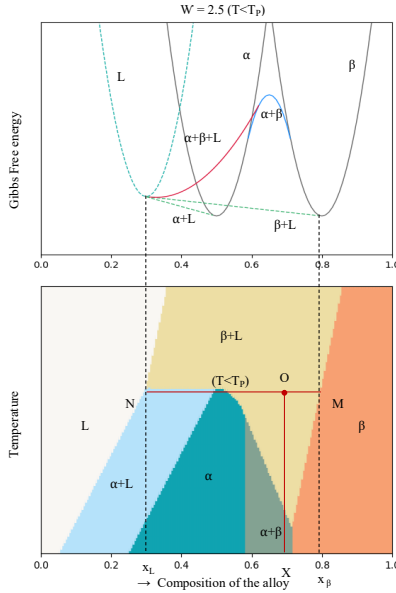


Figure 13: Application of lever rule on Peritectic phase equilibria map ( $\mathcal{W} = 2.5$ )

the black dashed line denotes the solidus boundary, representing the composition of the  $\beta$  phase ( $x_\beta$ ). The region between the two boundaries defines the two-phase  $\beta$ - $L$  field, where both phases coexist with compositions determined by the boundary lines at a given temperature.

In Figure 13, we can demonstrate the application of the lever rule below the peritectic temperature. To accomplish that, a point,  $O$ , is selected on the beta-liquid phase region, and a tie line,  $MN$ , is drawn across the phase equilibria map to determine the molar fraction of each phase extending from liquid to the solid beta phase. Our calculated compositions are approximately  $x_\beta = 0.7980$  for the beta phase and  $x_L = 0.2980$  for the liquid phase. Using Equation (19), we can determine the phase fractions for these phases; the molar fraction of solid phase  $\beta$  and the molar fraction of liquid ( $L$ ) can be written as follows:

$$z_\beta = \frac{X - x_L}{x_\beta - x_L} \quad (19a)$$

$$z_L = 1 - z_\beta \quad (z_\alpha = 0) \quad (19b)$$

## 5.6 Comparative Analysis with CALPHAD for Cu–Ag Alloy

Our model is analogized to the CALPHAD-derived phase diagram for the Cu–Ag binary alloy by comparing the calculated Gibbs free energies for the stable FCC phases. Specifically, the minimum Gibbs free energies obtained are 56,138.2 J/mol for the Ag FCC phase and  $-46,896.8$  J/mol for the Cu FCC phase. In our approach, we determine the Gibbs free energy for each phase by minimizing the free energy functions by adjusting the functions in equation 2 parameters to replicate these benchmark values. To include the effects of lattice mismatch, we calculate the coherency strain energy for three different strain levels—5%, 7.5%, and 10%—when Cu is epitaxially grown on an Ag substrate. The strain energy is calculated using Equation (5), where the coherency energy term  $g_e$  is incorporated into the total free energy of the system. This term accounts for the elastic energy associated with the misfit

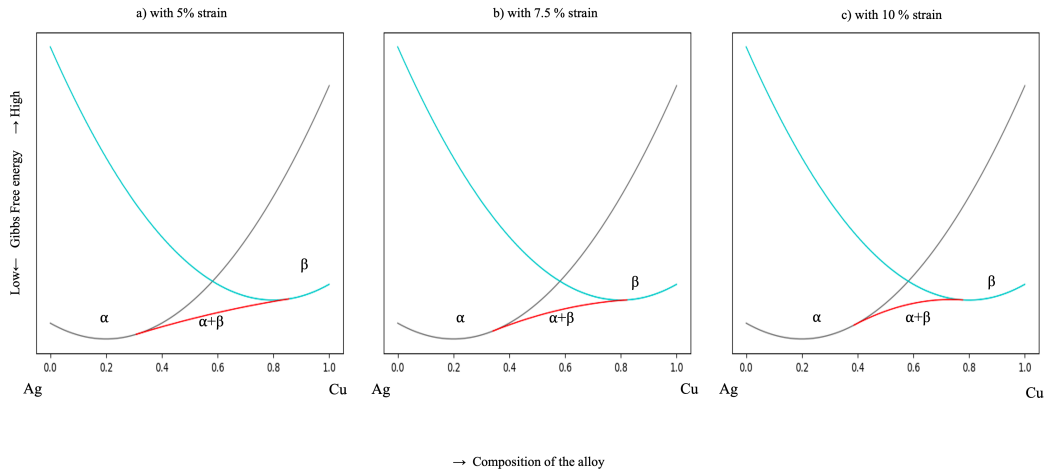


Figure 14: Comparative Analysis of the theoretical model for Cu–Ag Alloy

strain, which is especially important in systems where elastic contributions significantly affect phase stability. The coherency strain modifies the energy of the phases. As the strain increases, the overall Gibbs free energy of the Cu phase is modified by the additional elastic energy, leading to a shift in the free energy curves for the two-phase region,  $\alpha(\text{Ag})$ - $\beta(\text{Cu})$ . This change is reflected in our model by the deformation of the free energy surfaces, which in turn affects the common tangent construction. At higher strain levels, the two-phase region

predicted by the common tangent method becomes unstable. This instability, illustrated by the red curve in Figure 14, indicates that the strain-induced elastic energy dominates the chemical free energy difference between the phases, thereby suppressing the formation of a common tangent and indicating a strain-driven phase separation.

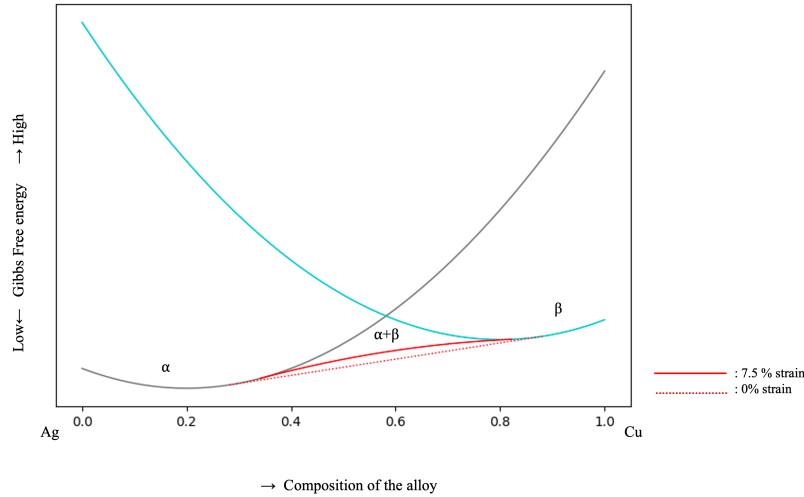


Figure 15: Deviation of stressed combination of phases vs non-stressed represented by tangent line

From the theoretical perspective, the approach is leveled in the interplay between chemical and elastic contributions to the Gibbs free energy. The CALPHAD method provides a robust baseline by accurately capturing the chemical free energy of the Cu–Ag system, while our model integrates the additional coherency strain effects. This combined framework is particularly forward-thinking because it moves beyond conventional CALPHAD by incorporating microstructural effects for a coherent alloy. In essence, the results highlight the importance of considering strain-induced modifications to the free energy when predicting phase equilibrium, a factor that is increasingly relevant in the design of advanced materials where mechanical constraints are intrinsic to the processing or application conditions.

Using the common-tangent construction, we establish a stress-free baseline and define the coherency penalty as the energy difference between the strained Cu–Ni curve and this baseline. Because when considering 5% strain due to copper’s lattice mismatch, its elastic

penalty is almost negligible. When we apply 7.5% strain, a clear bump appears in the energy curve, as shown in Figure 15 (solid red line) compared to the case without strain (dotted red line). This simple test confirms that our method isolates the elastic coherency contribution.

In summary, by parameterizing our model to get the CALPHAD-based chemical free energy and the additional elastic contributions from the coherency strain of Cu, we provide a comprehensive understanding of phase stability in the Cu–Ag system. This approach not only validates our model against established thermodynamic benchmarks but also offers predictive understandings of the coherent binary alloy for considerable importance in materials engineering.

## 6 Discussion

This study explores the eutectic and peritectic equilibrium in coherent binary alloys and provides insights into the phase behavior and stability under different coherency stress levels. We focus more on computational findings than on experimental ones, and all the parameters related to our phase equilibria maps, like composition, temperature, and coherency stress level, are considered arbitrary here. The following section discusses the implications and limitations of our findings, compares them with previous studies, and proposes directions for our future research.

In our study, we used Lagrange multipliers to investigate the effect of coherency stress on a binary alloy system for eutectic and peritectic equilibria. We considered a binary system rich in two solid phases and one liquid phase at higher temperatures. Through the computational approach, we found out how the coherency stress influenced the stability of those phases. We obtained stable phases and their associated compositions by minimizing the Gibbs free energy of the distinct phases over a specific range of temperatures, considering the element’s melting point differs from the invariant points, like eutectic and peritectic points. Furthermore, we looked at different levels of coherency stresses for the eutectic and peritectic phase equilibria. We considered infinite volume occupied by three phases to eliminate boundary effects, so the strain energy depends only on the phase mismatch and fractions, not on the size or shape of the systems. Furthermore, to isolate the effect of coherency strain without directional complexities, we consider our solid phases isotropic, exhibiting the same material properties in all directions and being linearly elastic. The

coherency energy invalidates the Gibbs rule along with the common tangent construction. The common tangent construction considers free energy separable from individual phase contributions, but elastic energy introduces a coupling between the phases. This coupling makes the phase compositions dependent on the overall composition and volume fractions, invalidating the common tangent method. Instead, equilibrium must be found by minimizing the total Gibbs free energy, including the elastic terms. In coherent solids, the common tangent construction is usually invalid as the free energy of the system is not simply the sum of the free energies of the individual phases independent of the position and morphology of the other phases. So, in our study, coherent phase equilibria maps can still be formulated by adding the elastic energy of the system to the free energies of the phases in the absence of deformation and then minimizing the resultant energy. [15]

Our computational model with the specific parameterized values discovered that under the coherency stress in a coherent binary alloy, the three-phase region,  $\alpha$ - $\beta$ - $L$  are formed in the eutectic case. At the same time, the peritectic equilibria show a distinct feature. The formation of this three-phase region in the eutectic and peritectic equilibria in a coherent binary alloy changes according to the extent of the coherency stress. The coherency stress level does not affect the formation of the three-phase region. Instead, it stabilizes the two-phase region ( $\beta$ - $L$ ) phase to be more dominant. The melting temperature of the solid phases,  $\alpha$ , and  $\beta$ , are similar in the case of the eutectic system, which forms the eutectic point.

In contrast, a peritectic point is created when the melting temperatures are significantly different. In the peritectic scenario, the  $\alpha$  phase has a lower melting point, making it unstable and unable to exist to withstand coherent stress. We used simplified quadratic functions Equations (17) and (18) to model this behavior and imitate the Gibbs energy curves. However, to simplify things, our three functions for  $\alpha$ ,  $\beta$ , and  $L$  are identical in shape but differ in composition. In the eutectic case, the liquid function is situated in the middle, whereas in the peritectic case, the liquid function appears at the sides. The eutectic point can be introduced by setting  $x_\alpha^0 < x_L^0 < x_\beta^0$ , whereas the peritectic point can be introduced by setting  $x_L^0 < x_\alpha^0 < x_\beta^0$ . Therefore, instead of forming the three-phase region,  $\alpha$ - $\beta$ - $L$ , the minimum Gibbs free energy of the  $\beta$ - $L$  becomes more dominant. In the result section, we explicitly stated how the changes are significant and how the rise in coherency stress levels results in the growth of the three-phase region  $\alpha$ - $\beta$ - $L$  in the eutectic phase equilibria. Additionally, we demonstrate how the two-phase region  $\beta$ - $L$  evolves dominant in

the peritectic phase equilibria.

In our research, we reference two earlier studies that described how the phase behaves under coherent conditions. Johnson and Voorhees worked with the complicated behavior of the eutectic equilibrium in coherent binary alloys, mainly focusing on the interaction between two solid phases under different thermodynamic conditions and how these interactions between the solid phases differ significantly from incoherent systems due to the influence of coherency strains and elastic stresses. In a separate but related study, Cahn and Larché explained a two-phase coherent system with a simple model to focus on the phase equilibrium affected by elastic energy contributions. They highlighted the impact of elastic energy on free energy and phase stability, challenging traditional methods of analyzing phase diagrams.

However, previous studies on coherent binary alloys have focused solely on the solid phases in eutectic equilibrium, with no investigation into the solid and liquid phases or the peritectic equilibrium. Our work adopts a novel approach by incorporating the liquid phase to examine the eutectic and peritectic equilibria of binary alloys by creating a model to minimize Gibbs energy using the Lagrange multipliers method, allowing us to determine the compositions of the phases over a range of temperatures. Nevertheless, our work is limited to some extent. When we consider the Gibbs energy function, the Gibbs energy function related to the liquid phase is only temperature-dependent, not the other two solid phases. Consequently, when subjected to stress, the solid phases do not experience a corresponding change thermodynamically in their melting point. In reality, the CALPHAD functions for each alloy phase are temperature-dependent, and the melting point should also vary. Our current research is restricted by the assumption of a temperature-dependent Gibbs energy function for the phases, which could be addressed in future studies.

## 7 Conclusion

The analysis applies the necessary conditions for thermal, mechanical, and interfacial equilibrium to determine phase equilibrium in a binary alloy considering infinite volume occupied by the phases, two solids, and one liquid, and considering the solid phases isotropic and linearly elastic. In the computational exploration of eutectic and peritectic equilibria in coherent binary alloys under varying coherency stress levels by utilizing Lagrange multipliers where the simplistic version of quadratic functions of Gibbs free energy have been considered subject to constraints for composition and volume fraction of two solid phases and one liquid phase following the preservation of mass representing the necessary conditions for the existence of a phase. We have identified unique phase behaviors and compositions that appear from the interactions between the solid phases as the reason for the coherence of the elements resulting from lattice mismatch. The goal is to find the compositions and molar fractions corresponding to all three phases in thermodynamic equilibrium or the eutectic and peritectic points. By assuming an infinite system, we eliminate boundary effects, so the strain energy depends only on the solid phase mismatch and fractions, not on the size or shape of the systems. Furthermore, to isolate the effect of coherency strain without directional complexities, we consider our solid phases isotropic, indicating the same material properties in all directions and being linearly elastic, so all results exclusively concern equilibrium phenomena.

Our results highlight the significant impact of coherency stresses on phase stability and composition in binary systems. It deduces the formation of the three-phase region,  $\alpha$ - $\beta$ - $L$  in eutectic equilibria, while the dominance of the two-phase region,  $\beta$ - $L$  over the three-phase region in peritectic equilibria has been observed. Our analysis found that due to the difference in the position of the solid and liquid function, referring to the composition, in the eutectic and peritectic case, these unique characteristics of the equilibria have been found, forming the three-phase region, the minimum Gibbs free energy of the two-phase region (solid and liquid) becomes more dominant. Moreover, the difference in the melting points of the solid phases is one reason behind observing how the changes are significant and how the rise in coherency stress levels results in the growth of the three-phase region in the eutectic phase equilibria. In contrast, the two-phase region evolves dominant under coherency stress in the peritectic phase equilibria.

However, the study identifies limitations in the current modeling approach, particularly

treating the Gibbs energy functions as temperature-dependent and not stress-responsive for the liquid phase. Our phase equilibria map, instead of the term 'phase diagram,' has been used in our study, which is the graphical representation showing phases in equilibrium under various conditions without detailing phase proportions, limited to the lever rule application. Our future research will aim to refine these models by including stress-dependent melting points and extending the Gibbs energy framework better to represent the thermodynamics of all phases under stress. This study can be implemented in strain engineering to investigate the role of elastic energy on phase stability in alloys. Future work will continue to clarify the subtle behaviors of materials for technology and engineering applications, causing the development of more robust alloys tailored to specific applications.

The present work advances previous studies of coherent binary alloys by incorporating the liquid phase with two solid phases. It shows that coherency stress alters phase compositions and influences phase stability differently in eutectic and peritectic systems, presenting an understanding of the complex interplay between thermodynamic and mechanical factors in alloy phase formation.

## References

- [1] W. D. Callister, D. G. Rethwisch, *Materials Science and Engineering: An Introduction*, 10th Edition, John Wiley & Sons, 2020.
- [2] D. A. Porter, K. E. Easterling, *Phase Transformations in Metals and Alloys* (Revised Reprint), 3rd Edition, CRC Press, 2009. doi:10.1201/9781439883570.
- [3] T. Massalski, Phase diagrams, in: *Encyclopedia of Materials: Science and Technology*, 2nd Edition, Elsevier, 2001, pp. 6842–6851. doi:10.1016/B0-08-043152-6/01214-6.
- [4] D. A. Porter, K. E. Easterling, M. Y. Sherif, *Phase Transformations in Metals and Alloys*, 4th Edition, CRC Press, 2021.
- [5] M. Lopuszyński, J. A. Majewski, Ordering in ternary nitride semiconducting alloys, *Physical Review B* 85 (5) (2011) 005111. doi:10.1109/PhysRevB.85.005111.  
URL <https://arxiv.org/abs/1108.2447>
- [6] G. B. Arfken, *Mathematical Methods for Physicists*, 3rd Edition, Academic Press, Orlando, FL, 1985, section on Lagrange Multipliers.
- [7] S. Lang, *Calculus of Several Variables*, Addison-Wesley, Reading, MA, 1973.
- [8] G. F. Simmons, *Differential Equations*, McGraw-Hill, New York, 1972.
- [9] D. Zwillinger (Ed.), *CRC Standard Mathematical Tables and Formulae*, 31st Edition, CRC Press, Boca Raton, FL, 2003, section on Lagrange Multipliers.
- [10] R. Schmid-Fetzer, Phase diagrams: The beginning of wisdom, *Journal of Phase Equilibria and Diffusion* 35 (2014) 735–760.
- [11] U. R. Kattner, The calphad method and its role in material and process development, *Tecnol. Metal. Mater. Min* 13 (2016) 3–15.
- [12] T. Massalski, Phase diagrams, in: *Encyclopedia of Materials: Science and Technology*, 2nd Edition, Elsevier, 2001, pp. 6842–6851.

- [13] M. Kamran, M. R. Fazal, *Renewable Energy Conversion Systems*, 2021.
- [14] L. C. Wang, Developing a thermodynamic model for the U-Pd-Rh-Ru quaternary system for use in the modelling of nuclear fuel.
- [15] W. Johnson, P. Voorhees, Coherent phase diagrams, *Bulletin of Alloy Phase Diagrams* 9 (3) (1988) 208–215.
- [16] A. P. A. Mustari, Y. Oka, M. Furuya, W. Takeo, R. Chen, 3d simulation of eutectic interaction of pb–sn system using moving particle semi-implicit (mps) method, *Annals of Nuclear Energy* 81 (2015) 26–33. doi:10.1016/j.anucene.2015.03.031.
- [17] A. Mohanbabu, M. Saravanan, J. Ajayan, S. Baskaran, Design and development of AlGa<sub>N</sub>/Ga<sub>N</sub> HEMT for biosensing applications for detection of cancers, tumors, and kidney malfunctioning, in: *Electronic Devices, Circuits, and Systems for Biomedical Applications: Challenges and Intelligent Approach*, Academic Press, London, UK, 2021, Ch. 5, pp. 95–114. doi:10.1016/B978-0-12-823000-1.00005-X.
- [18] D. P. Bertsekas, *Constrained Optimization and Lagrange Multiplier Methods*, 2nd Edition, Athena Scientific, 1996, revised edition.
- [19] R. F. Engle, A general approach to lagrange multiplier model diagnostics, *Journal of Econometrics* 20 (1) (1982) 83–104.
- [20] Z.-K. Liu, First-principles calculations and calphad modeling of thermodynamics, *Journal of Phase Equilibria and Diffusion* 30 (2009) 517–534.
- [21] J. Ågren, Calculation of phase diagrams: Calphad, *Current Opinion in Solid State and Materials Science* 1 (3) (1996) 355–360.
- [22] N. Saunders, A. P. Miodownik, *CALPHAD (Calculation of Phase Diagrams): A Comprehensive Guide*, Pergamon Materials Series, Pergamon, 1998, volume 1.
- [23] J. Cahn, F. Larché, A simple model for coherent equilibrium, *Acta metallurgica* 32 (11) (1984) 1915–1923.
- [24] S. Shi, J. Markmann, J. Weissmüller, Verifying larché–cahn elasticity, a milestone of 20th-century thermodynamics, *Proceedings of the National Academy of Sciences* 115 (43) (2018) 10914–10919.

- [25] B. Wang, L.-Q. Chen, Theory of strain phase equilibria and diagrams, *Acta Materialia* 274 (2024) 120025.
- [26] S. S. Behara, J. C. Thomas, B. Puchala, A. Van der Ven, Chemomechanics in alloy phase stability, *Physical Review Materials* 8 (3) (2024) 033801.
- [27] W. C. Johnson, P. Voorhees, Phase equilibrium in two-phase coherent solids, *Metallurgical Transactions A* 18 (1987) 1213–1228.
- [28] C. Chiang, W. C. Johnson, Coherent phase equilibria in systems possessing a consolute critical point, *Journal of Materials Research* 4 (3) (1989) 678–687.
- [29] R. Spatschek, G. Gobbi, C. Hüter, A. Chakrabarty, U. Aydin, S. Brinckmann, J. Neugebauer, Scale bridging description of coherent phase equilibria in the presence of surfaces and interfaces, *Physical Review B* 94 (13) (2016) 134106.
- [30] A. T. Phan, A. E. Gheribi, P. Chartrand, Coherent phase equilibria of systems with large lattice mismatch, *Physical Chemistry Chemical Physics* 21 (20) (2019) 10808–10822.
- [31] A. T. Phan, A. E. Gheribi, P. Chartrand, Modeling of coherent phase transformation and particle size effect in lifepo4 cathode material and application to the charging/discharging process, *Electrochimica Acta* 295 (2019) 632–644.
- [32] D. M. Wood, A. Zunger, Epitaxial effects on coherent phase diagrams of alloys, *Physical Review B* 40 (6).
- [33] A. G. Khachaturyan, *Theory of Structural Transformations in Solids*, Dover Publications, 2013.
- [34] H. Garcke, U. Weikard, Numerical approximation of the cahn-larché equation, *Numerische Mathematik* 100 (4) (2005) 639–662.
- [35] B. Bhadak, R. Sankarasubramanian, A. Choudhury, Phase-field modeling of equilibrium precipitate shapes under the influence of coherency stresses, *Metallurgical and Materials Transactions A* 49 (2018) 5705–5726.

- [36] C. Shen, J. Simmons, Y. Wang, Effect of elastic interaction on nucleation: Ii. implementation of strain energy of nucleus formation in the phase field method, *Acta materialia* 55 (4) (2007) 1457–1466.
- [37] A. L. Roytburd, G. Sung, The formation of epitaxial eutectic modulated structures, *MRS Online Proceedings Library (OPL)* 311 (1993) 143.
- [38] A. Deymier, P. A. Deymier, K. Muralidharan, M. Latypov, Thermodynamics of the solid-liquid phase equilibrium of a binary system: Effect of a chemical reaction in the liquid and epitaxial strain in the solid, *Acta Materialia* 259 (2023) 119299.
- [39] A. C. Deymier, P. A. Deymier, M. Latypov, K. Muralidharan, Effect of stress on the dissolution/crystallization of apatite in aqueous solution: a thermochemical equilibrium study, *Philosophical Transactions of the Royal Society A* 381 (2250) (2023) 20220242.